



저작자표시-비영리-변경금지 2.0 대한민국

이용자는 아래의 조건을 따르는 경우에 한하여 자유롭게

- 이 저작물을 복제, 배포, 전송, 전시, 공연 및 방송할 수 있습니다.

다음과 같은 조건을 따라야 합니다:



저작자표시. 귀하는 원저작자를 표시하여야 합니다.



비영리. 귀하는 이 저작물을 영리 목적으로 이용할 수 없습니다.



변경금지. 귀하는 이 저작물을 개작, 변형 또는 가공할 수 없습니다.

- 귀하는, 이 저작물의 재이용이나 배포의 경우, 이 저작물에 적용된 이용허락조건을 명확하게 나타내어야 합니다.
- 저작권자로부터 별도의 허가를 받으면 이러한 조건들은 적용되지 않습니다.

저작권법에 따른 이용자의 권리는 위의 내용에 의하여 영향을 받지 않습니다.

이것은 [이용허락규약\(Legal Code\)](#)을 이해하기 쉽게 요약한 것입니다.

[Disclaimer](#)

**Thesis for Degree of Master of Science**

**Model study on geochemical reactions  
in the reactive gas-groundwater-  
bentonite system under geological SNF  
repository conditions**

**by**

**Daehyun Shin**

**Division of Earth Environmental System Science**

**(Major of Earth and Environmental Sciences)**

**The Graduate School**

**Pukyong National University**

**February 2025**

Model study on geochemical reactions in  
the reactive gas-groundwater-bentonite  
system under geological SNF repository  
conditions

(사용 후 핵연료 지하 처분장 조건에서 반응성 가스-지하수-벤토나이트  
시스템의 지화학 반응 모델 연구)

Advisor: Prof. Minhee Lee

by

Daehyun Shin

A thesis submitted in partial fulfillment of requirements  
for the degree of Master of Science

Division of Earth Environmental System Science,  
(Major of Earth and Environmental Sciences)

The Graduate School

Pukyong National University

February 2025

Model study on geochemical reactions in  
the reactive gas-groundwater-bentonite  
system under geological SNF repository  
conditions

A thesis

by

Daehyun Shin

Approved by:

---

(Chairman) Sookyun Wang

---

(Member) YoungJae Kim

---

(Member) Minhee Lee

February 21, 2025

# CONTENTS

<b>CONTENTS</b> .....	<b>i</b>
<b>LIST OF FIGURES</b> .....	<b>iii</b>
<b>LIST OF TABLES</b> .....	<b>v</b>
<b>ABSTRACT</b> .....	<b>vi</b>
<b>CHAPTER 1. INTRODUCTION</b> .....	<b>1</b>
<b>CHAPTER 2. OBJECTIVES</b> .....	<b>5</b>
<b>CHAPTER 3. BACKGROUND</b> .....	<b>6</b>
3.1. Bentonite as the buffer material in the SNF repository .....	6
3.2. Geochemical reaction occurred in the SNF repository under hydrogeological evolution process .....	8
3.2.1. Generation of reactive gases CO <sub>2</sub> and H <sub>2</sub> S in the SNF repository....	9
3.2.2. Effects of reactive gases on bentonite as the buffer material .....	12
<b>CHAPTER 4. MODEL STUDY</b> .....	<b>15</b>
4.1. Geochemical reaction modeling to simulate the reactive gas-groundwater- bentonite system .....	15
4.1.1. Model domain and conditions .....	15
4.1.2. Geochemical reaction scenario for the modeling .....	17
4.1.2.1. Initial stage of the buffer zone .....	18
4.1.2.2. Geochemical reaction at redox environmental condition reaction stage .....	19
4.1.3. Properties of the bentonite used in the modeling .....	21

4.1.4. Water quality of the groundwater used in the modeling .....	23
4.1.5. Gas phase interaction in the modeling .....	25
4.1.6. Microbial activity in the modeling .....	26
4.1.7. Mineral dissolution and precipitation in the modeling .....	28
<b>CHAPTER 5. RESULTS AND DISCUSSION .....</b>	<b>33</b>
5.1. Equilibrium geochemical reaction modeling .....	33
5.1.1. Change of KURT groundwater quality at the equilibrium reaction modelling with atmospheric gases .....	33
5.2. Kinetic geochemical reaction modeling .....	35
5.2.1. Change of the KURT groundwater composition over the reaction time .....	35
5.2.2. Change of the gas concentration over reaction time .....	37
5.2.3. Change of the mineral composition in bentonite over the reaction time .....	40
5.2.4. Property changes of the Bentonil-WRK over the reaction time ....	45
<b>CHAPTER 6. CONCLUSIONS .....</b>	<b>48</b>
<b>REFERENCES .....</b>	<b>51</b>
<b>ACKNOWLEDGEMENTS .....</b>	<b>61</b>

## LIST OF FIGURES

Fig. 1. Global nuclear power generation in 2023 (from Ember-Energy Institute, 2024) .....	2
Fig. 2. Multi-barrier system of KBS-3 type for the SNF disposal (modified from POSIVA, 2020) .....	3
Fig. 3. The layer structure of montmorillonite (modified from Steinmetz, 2007) .....	7
Fig. 4. Schematic of the THM (thermo-hydro-mechanical) coupled processes in the multi-barrier system (modified from Lee et al., 2020).....	8
Fig. 5. Geochemical reactions occurred in the engineering barrier of the SNF repository site .....	13
Fig. 6. Schematic of the radionuclide migration changes in the buffer material due to geochemical reactions .....	14
Fig. 7. Schematic representation of the copper canister, buffer material, technical gaps and host rock illustrating the model domain (modified from Hung et al., 2023) .....	16
Fig. 8. Modeling scenarios for the early stage of the SNF repository based on the hydrogeological evolution process after the SNF disposal .....	18
Fig. 9. Modeling scenarios for the kinetic geochemical reactions in the buffer zone due to the hydrogeological evolution process for modeling .	20
Fig. 10. Result of the XRD analysis of the Bentonil-WRK .....	22
Fig. 11. Modeling results of KURT groundwater pH and pe changes over 10,000 years .....	36
Fig. 12. Results of changes in the initial groundwater oxygen concentration (a) and the concentration of atmospheric gases (b) .....	37

Fig. 13. Results of changes in the concentration of atmospheric gases .....	38
Fig. 14. Results of modeling for the concentration changes of the generated H <sub>2</sub> S gas .....	38
Fig. 15. Results of modeling for the mass changes of montmorillonite in bentonite over 100,000 reaction years (Right: 10,000 years) .....	41
Fig. 16. Results of modeling for the mass change of calcite in bentonite over 100,000 reaction years (Right: 1,000 years) .....	41
Fig. 17. Results of modeling for the mass change of kaolinite over 100,000 reaction years (Right: 10,000 years) .....	43
Fig. 18. Results of modeling for the mass change of chalcedony over 100,000 years .....	43
Fig. 19. Results of modeling for the mass change of dolomite over 100,000 years (Right: 1,000 year) .....	44
Fig. 20. Results of modeling for the mass change of pyrite over 100,000 years (Right: 10,000 years) .....	45
Fig. 21. Results of modeling for the change in bentonite properties over 100,000 years (Bottom: 100 years) .....	47

## LIST OF TABLES

Table 1. Reaction equations of CO <sub>2</sub> and H <sub>2</sub> S gas generation in SNF repositories .....	11
Table 2. Result of XRF analysis for the Bentonil-WRK .....	22
Table 3. Characteristics of groundwater sample at DB-3 site in the KURT (KAERI) .....	24
Table 4. Reaction equations for microbial decomposition of organic matter used in the modeling .....	27
Table 5. Parameters for microbial oxidation and reduction kinetics in the modeling .....	27
Table 6. Results of quantitative XRD analysis (wt%) for mineral constituents in the Bentonil-WRK(Cha et al., 2023) .....	29
Table 7. Thermodynamic constants of bentonite constituent mineral and secondary mineral used in the modeling at 60°C .....	29
Table 8. Kinetic reaction modeling parameters of the bentonite minerals applied in this modeling .....	31
Table 9. Kinetic reaction modeling parameters of the secondary precipitation minerals applied in this modeling .....	32
Table 10. Adjusted KURT groundwater quality after the geochemical reaction modeling .....	34
Table 11. Changes in the partial pressure of atmospheric gases after initial KURT groundwater-Atmosphere equilibrium modeling .....	35
Table 12. Results of changes in atmospheric partial pressure over 100,000 years .....	39

# Model study on geochemical reactions in the reactive gas-groundwater-bentonite system under geological SNF repository conditions

Daehyun Shin

Division of Earth Environmental System Science

(Major of Earth and Environmental Sciences)

The Graduate School

Pukyong National University

## Abstract

Bentonite is widely recognized as a key buffer material in spent nuclear fuel (SNF) repositories due to its high swelling capacity, low hydraulic conductivity, and high radionuclide adsorption properties. However, reactive gases such as CO<sub>2</sub> and H<sub>2</sub>S, generated during the hydrogeological evolution process of the SNF repository, can alter chemical and physical properties of the buffer material (Bentonite), potentially impacting the long-term stability of the repository. In this study, the long-term geochemical reaction modeling was conducted to evaluate the effects of reactive gases (CO<sub>2</sub> and H<sub>2</sub>S) on the properties of the bentonite (Bentonil-WRK), one of candidate buffer materials for the domestic SNF repository. Geochemical reaction modeling was performed to simulate the reactive gas-groundwater-bentonite reaction system using PHREEQC version 3.7.3, geochemical reaction code with the LLNL (Lawrence Livermore National Laboratory) database as the thermodynamic data source. Mineralogical properties of the Bentonil-WRK and water quality data of the KURT (KAERI Underground Research Tunnel) groundwater sample were used in this model study. Reaction of gases in the aqueous system, microbial respiration at redox condition, and mineral dissolution/precipitation in bentonite were mainly considered as geochemical reactions in this modeling process.

Equilibrium modeling results showed that infiltrating groundwater from the host

rock transitioned to an acidic and aerobic environment in the buffer zone due to the dissolution of residual atmospheric gases in pore spaces of the bentonite block. Subsequently, microbial respiration consumed  $O_2$  and  $SO_4^{2-}$  ions in pore water at redox conditions, generating  $CO_2$  and  $H_2S$  gases. The aerobic environment in the buffer zone was transitioned to the anaerobic condition after approximately 5,190 years of aerobic microbial reaction. As primary minerals in the Bentonil-WRK, montmorillonite and calcite showed mass losses of 0.024% and 0.37%, respectively, during the dissolution process, which led to the precipitation of secondary minerals such as kaolinite, dolomite, chalcedony, and pyrite. Over the 100,000-year simulation period, mineral volume in the bentonite decreased by 0.0029%, and pore volume of the Bentonil-WRK increased by 0.0043%. These results indicate that dissolution reactions were dominant throughout the 100,000-year geochemical reaction period and suggest that the reactive gases potentially generated in the SNF repository environment can alter the properties of the buffer material at the SNF repository.

Key words: Bentonil-WRK, Bentonite, Buffer, Geochemical reaction, Geochemical reaction modeling, Reactive gases, SNF repository

## CHAPTER 1. INTRODUCTION

Continuous use of fossil fuels has led to the generation of greenhouse gases like carbon dioxide (CO<sub>2</sub>), methane (CH<sub>4</sub>), and nitrous oxide (N<sub>2</sub>O), which are major contributors to the global warming (Brook et al., 2014). To address these climate changes, action plans such as the United Nations Framework Convention on Climate Change (UNFCCC) has mandated the reduction of greenhouse gas emissions in 2015(Mathew, 2022). In order to reduce greenhouse gas emissions, the use of renewable energy sources such as solar power, wind power, and nuclear power have been actively considered. Nuclear power plants produce extremely low CO<sub>2</sub> emissions, only 10-15 g of CO<sub>2</sub> per kilowatt-hour of electricity generated, making it a low-carbon energy source (Bruckner et al., 2014). Nuclear power generates electricity from the energy produced when an atom is split into two or more(Schunck and Regnier, 2022). The primary fuel used in nuclear power generation is U-235, and the heat energy released during nuclear fission is converted to the electrical energy. As of 2023, nuclear power generation constitutes a significant portion of electricity production in countries such as the United States (775.35 TWh), China (434.72 TWh), France (335.65 TWh), Russia (217.47 TWh), and South Korea (180.49 TWh) (Fig. 1) (Ritchie et al., 2024). South Korea produces the 5th largest amount of nuclear energy in the world (Ember 2024).

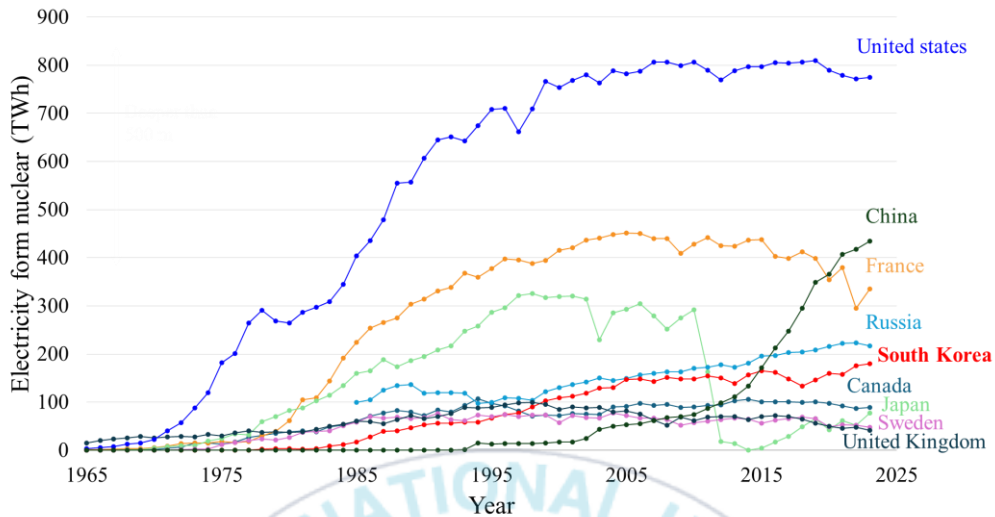


Fig. 1. Global nuclear power generation in 2023 (from Ember-Energy Institute, 2024).

However, nuclear power generation has the significant drawback of producing radioactive waste. Radioactive waste refers to any material contaminated with or containing detectable levels of radioactive substances above the established thresholds. Radioactive waste is broadly divided into two categories: the low and intermediate-level radioactive waste (LLW and ILW) and the high-level radioactive waste (HLW) (Deng et al., 2020). Waste with a half-life longer than 20 years, emitting alpha radiation, a radioactivity concentration exceeding 4,000 Bq/g, and a heat generation rate above 2 kW/m<sup>3</sup> is classified as the HLW. All other radioactive waste is categorized as LLW or ILW (Kim et al., 2023a). Most HLW consists of spent nuclear fuel (SNF) and, due to its high heat generation and radioactivity levels, is considered a special type of radioactive wastes (IAEA, 1994). South Korea currently has no facilities for the permanent storage of the HLW generated by the operation of nuclear power plants. As a result, this waste is stored in temporary storage facilities on the ground. However, these temporary facilities have limited capacity, which is insufficient for the permanent storage of the continuously generated SNF. Plans are now underway to construct

permanent storage facilities for SNF, and the deep geological repositories (DGRs) are widely recognized as the permanent storage solution for SNF worldwide (IAEA, 2003). The DGRs consist of a multi-barrier system based on the KBS-3 concept developed by the Swedish SKB (SKB, 2010), which includes an engineered barrier system (EBS) consisting of metallic storage canisters, buffer materials, and backfill materials, and the natural barrier system (NBS) consisting of the surrounding host rock. These repositories are typically located at depths greater than 500 meters for the leakage safety. (Zheng et al., 2015) (Fig. 2).

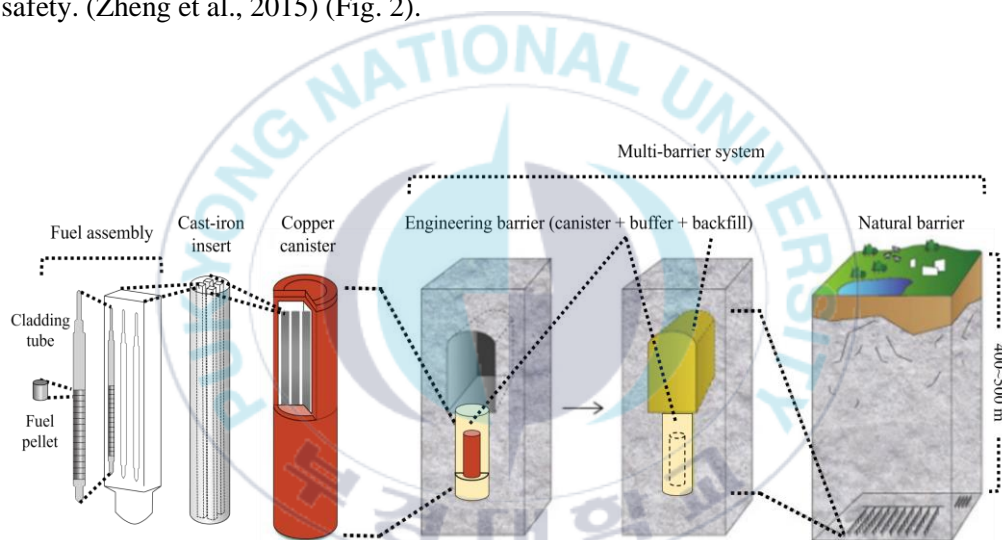
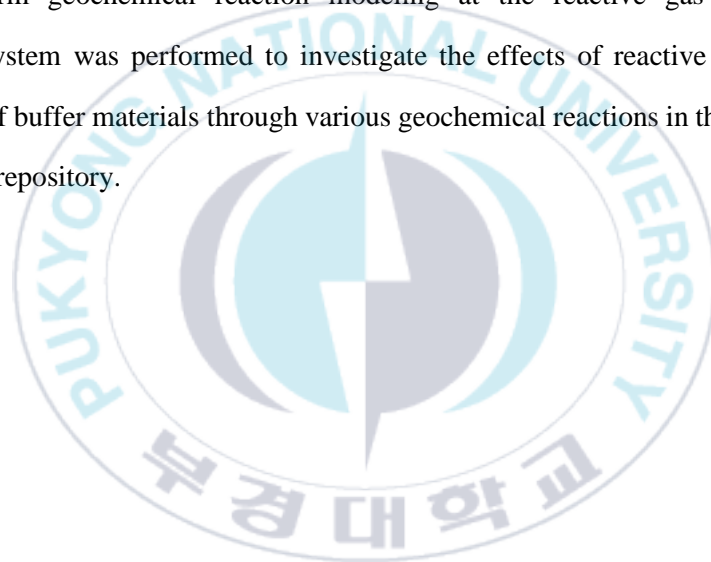


Fig. 2. Multi-barrier system of KBS-3 type for the SNF disposal (modified from POSIVA, 2020).

In South Korea, the Korean Reference Disposal System (KRS), based on the KBS-3 concept was designed for a granite host rock at first (Lee et al., 2007). Subsequently, the enhanced Korean Reference Disposal System (KRS+), optimized for the Korean landfill concept, was proposed and has since been adopted as the standard for the domestic SNF disposal facility (Lee et al., 2020b).

After the closure of the SNF repository, various geochemical reactions may occur during the hydrogeological evolution process of the repository, such as the generation of reactive gases, biochemical reactions and the corrosion of canisters. Reactive gases could be generated by microbial respiration and/or the corrosion of canisters. These gases can dissolve in groundwater, potentially altering water quality, dissolving buffer materials and forming secondary precipitated minerals, thereby influencing the behavior of leaked radionuclides in the multi-barrier of the SNF repository. In this study, the long-term geochemical reaction modeling at the reactive gas-groundwater-bentonite system was performed to investigate the effects of reactive gases on the properties of buffer materials through various geochemical reactions in the buffer zone of the SNF repository.



## CHAPTER 2. OBJECTIVE

The objective of this study is to investigate the effects of reactive gases on the properties of bentonite (Bentonil-WRK) in the buffer zone through the long-term geochemical reaction modeling, evaluating the safety of the bentonite (Bentonil-WRK) as the buffer materials in the SNF repository.

From the long-term modeling study, quantitative results for changes in properties of the buffer material by the geochemical reactions with reactive gases would be provided and the long-term interactions among gas, radioactive nuclide, bentonite, and groundwater could be understood in greater detail.

## CHAPTER 3. BACKGROUND

### 3.1. Bentonite as the buffer material in the SNF repository

As one of the engineered barrier systems in the SNF repository, the buffer serves to protect the copper canister from physical impacts from the environment, to delay groundwater inflow from the surrounding bedrock, and to minimize radionuclide migration if the copper canister loses function and radionuclides are released (Sun et al., 2020). Bentonite is considered as a potential buffer material due to its large specific surface area, high cation exchange capacity, high swelling capacity, and low hydraulic conductivity (Fernández et al., 2014). Bentonite is composed mainly of montmorillonite belong to the smectite group, which is a silicate clay mineral formed with two tetrahedral silicon ion sheets and one octahedral aluminum ion sheet (2:1 structure). The interlayer spaces in a montmorillonite contain exchangeable cations such as  $\text{Ca}^{2+}$ ,  $\text{Na}^+$ , and  $\text{K}^+$  (Fig. 3).

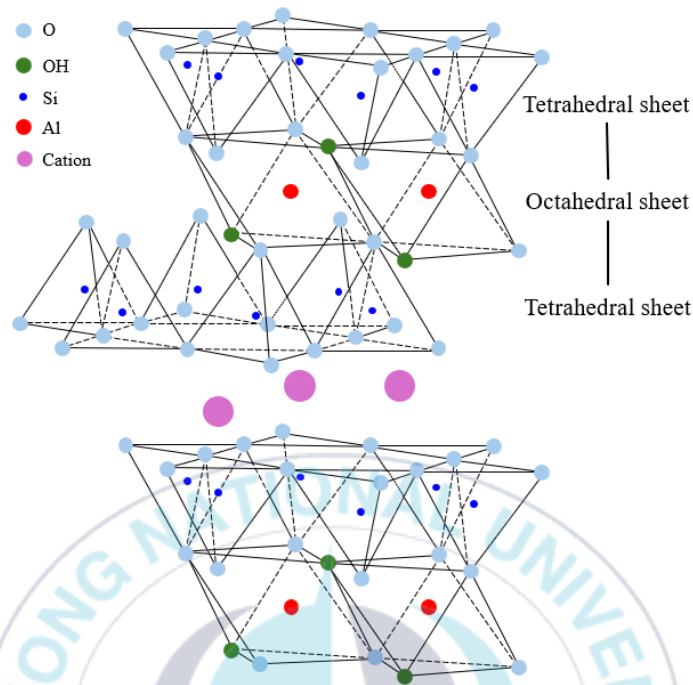


Fig. 3. The layer structure of montmorillonite (modified from Steinmetz, 2007).

The type of bentonite is determined by major exchangeable cations ( $\text{Na}^+$  and  $\text{Ca}^{2+}$ ) present between the inter layers of montmorillonite, and the most common types are the Ca-type and the Na-type bentonite. Depending on the geochemical conditions during its formation, bentonite may contain various accessory minerals, including quartz, feldspar, gypsum, calcite, and pyrite. Significant amounts of amorphous materials and organic compounds may also be present in the bentonite (Karlund, 2010). Various types of bentonite are being investigated worldwide as the buffer material in the SNF repository, such as MX-80 (Jalique et al., 2016), FEBEX (Wilson, 2017) and GMZ bentonite (Ye et al., 2009) being notable examples. In South Korea, “Bentonil-WRK (purchased from Clariant Korea)” is being considered as a buffer material for the enhanced Korean Standard Disposal System (KRS+). The chemical and mineralogical composition of the Bentonil-WRK is presented in chapter 4.

### 3.2. Geochemical reactions occurred in the SNF repository under hydrogeological evolution process

Geochemical reactions with various mechanisms can occur in the SNF repository, related to the evolution of the hydrogeological environment. A variety of geochemical reactions, deeply involved with heat generated by the canister, groundwater supported from the surrounding host rock, leached ions due to canister corrosion, and microbial respiration, can induce a variety of thermal, hydrological, mechanical, and chemical (THMC) changes in the multi-barrier. These changes have the potential to affect the long-term migration of the radioactive nuclide and the property of the bentonite buffer (Lee et al., 2019) (Fig. 4).

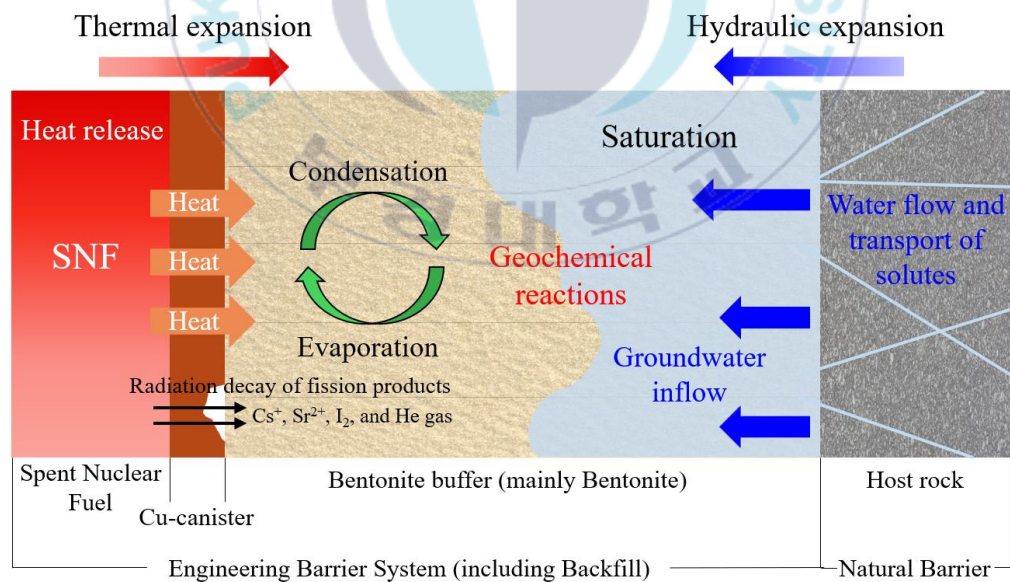


Fig. 4. Schematic of the THM (thermo-hydro-mechanical) coupled processes in the multi-barrier system (modified from Lee et al., 2020a).

Research on various geochemical reactions in SNF repositories is being conducted using a variety of methods, including laboratory-scale experiments, numerical migration modeling and geochemical reaction modeling. Mineralogical studies related to chemical reactions with the bentonite as a buffer material have focused on interactions such as bentonite-concrete and bentonite-canister reactions (Fernandez et al., 2009; Marty et al., 2010). In addition, various studies have been conducted on biological reactions, including oxygen consumption and sulfate reduction due to respiration by microorganisms present in the repository (Hung et al., 2023; Kim et al., 2023b). However, few studies have been conducted for the long-term stability of the bentonite buffer due to reactive gases that may generate in the SNF repository.

### 3.2.1. Generation of reactive gases CO<sub>2</sub> and H<sub>2</sub>S in the SNF repository

The generation of reactive gases in the SNF repository is primarily caused by corrosion of the canister and decomposition of organic matter by microbial respiration (Bond et al, 1997; Wikramaratna et al, 1993). The CO<sub>2</sub> gas and H<sub>2</sub>S gas are typical of the reactive gases that may be generated in SNF repository. The CO<sub>2</sub> gas is a common reactive gas generated by the decomposition of organic carbon by microbial respiration in aerobic and anaerobic environments. The H<sub>2</sub>S gas can be generated by dormant sulfate-reducing bacteria that become active and reduce sulfate as the SNF repository environment evolves, consuming oxygen and transitioning to an anoxic environment. The H<sub>2</sub>S gas can also be generated by the anaerobic corrosion of canister. The microbial activity as the main mechanism of gas generation, has been investigated in several previous studies, and its roles in processes such as canister corrosion, clay mineral alteration, gas production, and the mobility of radioactive nuclides have been also studied (Bagnoud et al., 2016; Meleshyn, 2014; Ruiz-Fresneda et al., 2023). The

presence of microorganisms inhabiting in repository sites and groundwater has also been reported in several studies (West et al., 1985; Jain et al., 1997). Microorganisms present in the surrounding host rock and groundwater can be drawn into the bentonite buffer by the inflow of groundwater, and the high expansion property of bentonite leaves insufficient space for microbial activity, reducing the activity of viable microorganisms in pore spaces of the bentonite buffer (Pedersen, 2000). However, natural microorganisms may show greater resistance in high-temperature and high-pressure environments (Mulligan et al., 2009). The  $\text{HS}^-$  ion may exist naturally in groundwater or may be produced by sulfate-reducing bacteria (SRB). The produced  $\text{HS}^-$  can be adsorbed on copper storage vessels and accelerate the corrosion of the storage vessel. This process can result in the formation of  $\text{H}_2\text{S}$  gas (King et al., 2013; King et al., 2021). The mechanisms of  $\text{CO}_2$  gas and  $\text{H}_2\text{S}$  gas generated by microbial respiration in the buffer and corrosion reactions in the copper canister are shown in Table 1.

Table 1. Reaction equations of CO<sub>2</sub> and H<sub>2</sub>S gas generation in SNF repositories.

Mechanism		Reaction equation
Microbial respiration	Aerobic respiration	$\text{CH}_2\text{O} + \text{O}_2 = \text{CO}_2 + \text{H}_2\text{O}$ $\text{C}_6\text{H}_{12}\text{O}_6 + 6\text{O}_2 = 6\text{CO}_2 + 6\text{H}_2\text{O}$ $\text{CH}_3\text{COOH} + 2\text{O}_2 = 2\text{CO}_2 + 2\text{H}_2\text{O}$
	Denitrification	$5\text{C}_6\text{H}_{12}\text{O}_6 + 24\text{NO}_3^- + 24\text{H}^+ = 30\text{CO}_2 + 12\text{N}_2 + 42\text{H}_2\text{O}$ $5\text{CH}_3\text{COOH} + 8\text{NO}_3^- + 8\text{H}^+ = 10\text{CO}_2 + 4\text{N}_2 + 14\text{H}_2\text{O}$ $\text{CH}_3\text{COOH} + 4\text{NO}_3^- = 2\text{CO}_2 + 4\text{NO}_2^- + 2\text{H}_2\text{O}$ $3\text{CH}_3\text{COOH} + 8\text{NO}_2^- + 8\text{H}^+ = 6\text{CO}_2 + 4\text{N}_2 + 10\text{H}_2\text{O}$
	Sulfate reduction	$2\text{CH}_2\text{O} + \text{SO}_4^{2-} + \text{H}^+ = 2\text{CO}_2 + \text{HS}^- + 2\text{H}_2\text{O}$ $\text{CH}_3\text{COOH} + \text{SO}_4^{2-} + 2\text{H}^+ = \text{H}_2\text{S} + 2\text{CO}_2 + 2\text{H}_2\text{O}$
Cu-canister corrosion	Anodic reaction	$\text{Cu} + \text{HS}^- = \text{Cu}(\text{HS})_{\text{ADS}} + \text{e}^-$ $\text{Cu} + \text{Cu}(\text{HS})_{\text{ADS}} + \text{HS}^- = \text{Cu}_2\text{S} + \text{H}_2\text{S} + \text{e}^-$

\*ADS: Adsorption

### 3.2.2. Effects of reactive gases on bentonite as the buffer material

Reactive gases such as CO<sub>2</sub> and H<sub>2</sub>S that may be generated in the SNF repository and dissolve in groundwater, causing pH changes and triggering mineral dissolution and precipitation in buffer. The most significant effect of reactive gases is the lowering of the pH of infiltrating groundwater, which can change the buffer environment to acidic condition. Reaction by which the CO<sub>2</sub> gas decreases the pH of groundwater is as follows:



The CO<sub>2</sub> gas dissolves in water (Eq. 1), forming the H<sub>2</sub>CO<sub>3</sub> ions (Eq. 2). Subsequently, H<sup>+</sup> ions are dissociated from the carbonic acid, forming HCO<sub>3</sub><sup>-</sup> ions (Eq. 3), and further dissociation of H<sup>+</sup> ions result in the formation of CO<sub>3</sub><sup>2-</sup> ions (Eq. 4). Through this series of reactions, the CO<sub>2</sub> gas can alter groundwater quality to a more acidic environment (Mitchell., et al 2010). The reaction by which the H<sub>2</sub>S gas decreases the pH of groundwater is as follows:



The H<sub>2</sub>S gas dissolves in water, forming the H<sub>2</sub>S ions (Eq. 5). The H<sup>+</sup> ions are dissociated, forming HS<sup>-</sup> ions (Eq. 6), and further dissociation results in the formation

of  $S^{2-}$  ions (Eq. 7). Through this series of reactions, groundwater quality can be altered to an acidic environment. If the  $CO_2$  gas is continuously produced and the partial pressure exceeds atmospheric conditions, the pH of groundwater will decrease and mineral like calcite in bentonite may start to dissolve (Itäla et al., 2013). The  $H_2S$  gas is able to move relatively freely in the buffer medium, allowing it to pass through a variety of micropores and to actively participate in the buffer medium (Wersin et al., 2014). Typical geochemical reactions related to reactive gases such as  $CO_2$  and  $H_2S$  occurred around the buffer at the SNF repository environment are shown in Fig. 5.

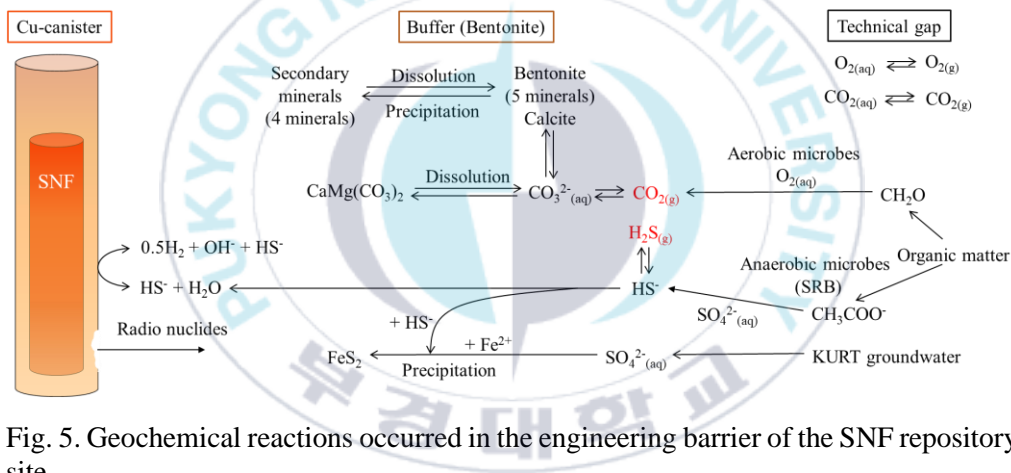


Fig. 5. Geochemical reactions occurred in the engineering barrier of the SNF repository site.

These various geochemical reactions can alter the properties of the buffer material, such as the dissolution of bentonite constituents and the formation of secondary precipitated minerals. Such changes in properties can also affect the behavior of leaked radionuclides and gases in the buffer, potentially affecting the long-term stability of the SNF repository (Fig. 6).

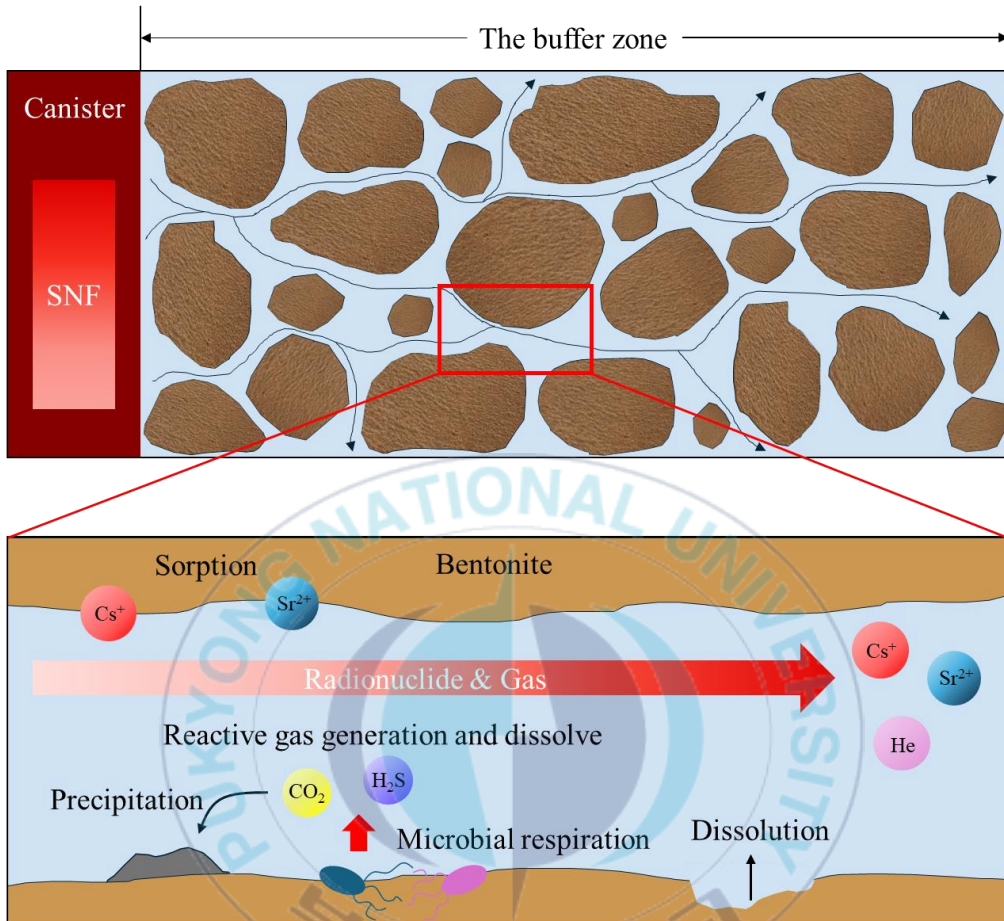


Fig. 6. Schematic of the radionuclide migration changes in the buffer material due to geochemical reactions.

## CHAPTER 4. MODEL STUDY

### 4.1. Geochemical reaction modeling to simulate the reactive gas-ground water-bentonite system

The geochemical reaction modeling was performed using by PHREEQC (version 3.7.3), a software developed by the U.S Geological Survey (USGS) (Parkhurst and Appelo, 2013). The thermodynamic database was obtained from the Lawrence Livermore National Security (LLNL) database (Wolery and Sutton, 2013).

#### 4.1.1. Model domain and conditions

The model domain for geochemical reaction modeling was restricted to the saturated buffer zone with the implementation of the concept of a vertical disposal in a SNF repository. The buffer zone was composed of the compacted bentonite blocks having technical gaps at block boundaries and at the wall surface between the block and the host rock. Geochemical reaction modeling was performed under the assumption that groundwater from the surrounding natural bedrock would completely saturate the technical gaps as well as pore spaces in the buffer zone (Fig. 7). Furthermore, the modeling was conducted under conditions which are a temperature of 60°C and a pore pressure of 5 MPa, representing the state when the technical gap and buffer zone are completely saturated with groundwater at the subsurface SNF repository.

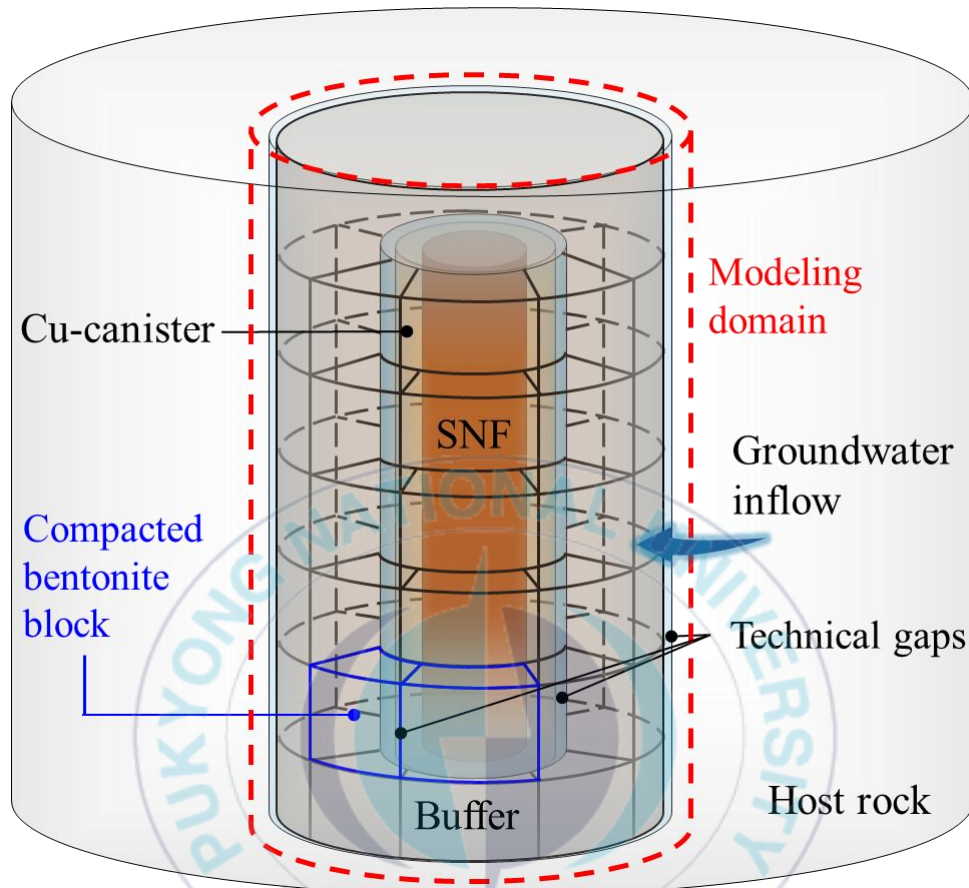


Fig. 7. Schematic representation of the copper canister, buffer material, technical gaps and host rock illustrating the model domain (modified from Hung et al., 2023).

#### 4.1.2. Geochemical reaction scenario for the modeling

The evolution of the hydrogeologic environment around the repository site after the closure of a spent nuclear fuel (SNF) storage may give rise to a variety of geochemical reactions in the buffer zone. In this modeling study, three geochemical reactions were mainly considered at the reactive gas-groundwater-bentonite system; ① reactive gas-groundwater reaction in equilibrium condition, ② kinetic microbial respiration at aerobic and anaerobic condition, and ③ kinetic mineral dissolution and precipitation of the bentonite. The geochemical reaction modeling conducted in this study can be categorized into two scenarios to simulate the property change of the bentonite buffer over the reaction time.

1. First stage of the SNF repository: Following the closure of the SNF storage at the repository, the groundwater inflow from the surrounding bedrock begins. During the construction of the SNF repository, the atmospheric constituent gases inflow and were trapped in pores of the buffer zone subsequently. These gases later dissolve in the inflowing groundwater, leading to a state of equilibrium between reactive gas and groundwater.
2. Second stage of the SNF repository: After the SNF repository is fully saturated with groundwater, the microbial activity may occur under aerobic environmental conditions, generating more gases and controlling dissolution-precipitation reactions. This is followed by anaerobic microbial respiration and dissolution-precipitation reactions of bentonite constituent minerals even after complete depletion of oxygen in the reservoir for a long time.

#### 4.1.2.1 Initial stage of the buffer zone

In the early stage of the SNF repository, the repository site is exposed to open atmospheric conditions, and this exposure maintains the SNF repository environment to aerobic conditions (Acero et al., 2010). As the SNF repository is closed, the void spaces of bentonite buffer contain trapped atmospheric constituent gases, including reactive gases such as  $O_2$  and  $CO_2$ . Subsequently, as groundwater flows in from the surrounding bedrock, the atmospheric gases present in the voids are partially or completely dissolved in groundwater, and dissolved oxygen ions and carbonic acid and bicarbonate ions are formed in groundwater, changing the composition of groundwater. As a result, the initial phase of the buffer system becomes aerobic and acidic (Fig.8).

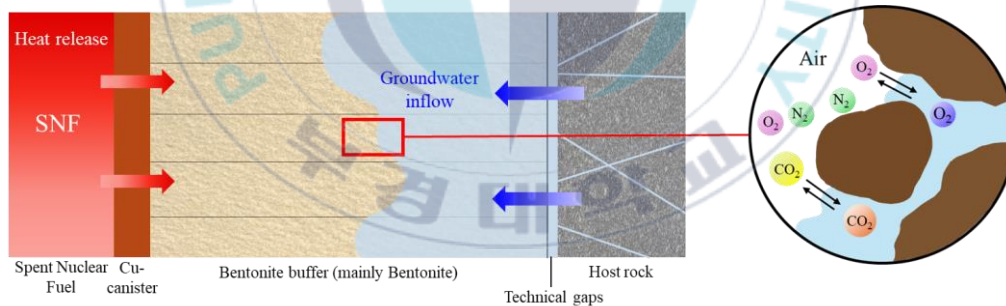


Fig. 8. Modeling scenarios for the early stage of the SNF repository based on the hydrogeological evolution process after the SNF disposal.

The saturation of the interior of the buffer zone with infiltrating water was estimated to take approximately 250 years and the maximum pressure in the cavities is expected to reach 3 to 5 MPa at the time of infiltration. The temperature of the bentonite buffer material varies depending on the subsurface geological environment, storage hole arrangement method, etc., but it gradually decreases from a maximum of 87.3°C at the beginning of repository closure and reaches a temperature of about 26.6°C after

100,000 years (Kim et al., 2021). Equilibrium between groundwater and atmospheric gas was assumed at an initial stage of the buffer zone, at a pore pressure and temperature conditions of 5 MPa and 60°C respectively.

#### 4.1.2.2 Geochemical reaction at redox environmental condition reaction stage

In the fully saturated with groundwater and in equilibrium with atmospheric constituent gases, respiration reactions of aerobic microorganisms using oxygen ions as electron donors occur in buffer zone as well as dissolution-precipitation reactions. The dissolution of organic carbon in bentonite into groundwater and the decomposition of organic carbon by the respiration of microorganisms at aerobic condition result in the additional production of CO<sub>2</sub> gas. When the bentonite buffer becomes saturated and swells, the pore size becomes smaller than that of the microorganisms, so it is assumed that microbial reactions mainly occur in the technical gaps where microorganisms can still be relatively active. The modeling is performed by assuming that the dissolution-precipitation reaction of minerals in bentonite also occurs simultaneously. Then, when the oxygen is completely consumed and the environment is changed from aerobic to anaerobic, H<sub>2</sub>S gas and CO<sub>2</sub> gas are additionally produced in the process of decomposition of organic carbon by the respiration of microorganisms using sulfate as an electron donor. As a result, the kinetic geochemical reaction has been going on for 100,000 years in this model (Fig. 9).

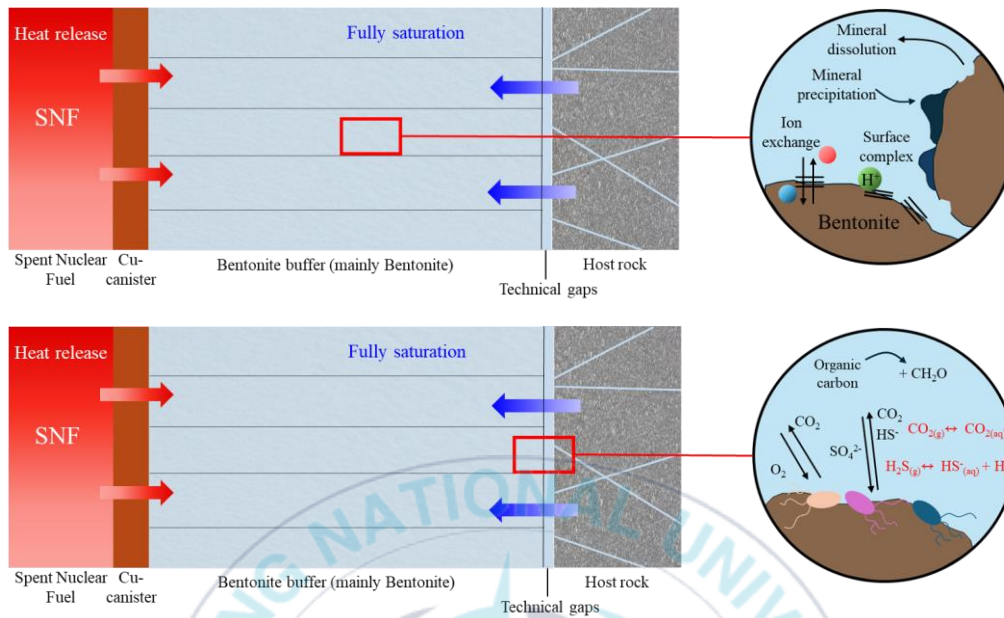


Fig. 9. Modeling scenarios for the kinetic geochemical reactions in the buffer zone due to the hydrogeological evolution process for modeling.

#### 4.1.3. Properties of the bentonite used in the model study

The bentonite considered in the model study was the Bentonil-WRK, which was very strong candidates for a buffer material in the South Korea repository site. Bentonil-WRK, has been manufactured by the Clariant Korea Corporation and supplied by the KAERI (Korea Atomic Energy Research Institute). The X-ray diffractometer (XRD; PANalytica, X'Pert3-powder) and X-ray fluorescence (XRF; Rigaku, ZSX-PrimusIV) analyses were performed to determine its chemical and mineralogical characteristics before the model study. From XRF and XRD analyses, the Bentonil-WRK was composed of SiO<sub>2</sub> (64.47%), Al<sub>2</sub>O<sub>3</sub> (18.05%), Fe<sub>2</sub>O<sub>3</sub> (5.23%), and CaO (5.98%) (Table 2). The high SiO<sub>2</sub> and Al<sub>2</sub>O<sub>3</sub> contents of the bentonite were attributed to the 2:1 layered structure of silica tetrahedra and aluminum octahedra in the montmorillonite, and the Bentonil-WRK was classified as a Ca-type bentonite, because of high CaO contents in the XRF result. The XRD analysis revealed distinct peaks of minerals like montmorillonite and albite, along with additional peaks of cristobalite, quartz, and calcite as accessory minerals (Fig. 10).

Table 2. Result of XRF analysis for the Bentonil-WRK

Composition	Wt (%)
Na <sub>2</sub> O	0.71
MgO	2.85
Al <sub>2</sub> O <sub>3</sub>	18.05
SiO <sub>2</sub>	64.47
P <sub>2</sub> O <sub>5</sub>	0.19
SO <sub>3</sub>	0.18
K <sub>2</sub> O	1.42
CaO	5.98
TiO <sub>2</sub>	0.77
MnO	0.11
Fe <sub>2</sub> O <sub>3</sub>	5.23
SrO	0.02
Etc.	0.04
Total	100.00

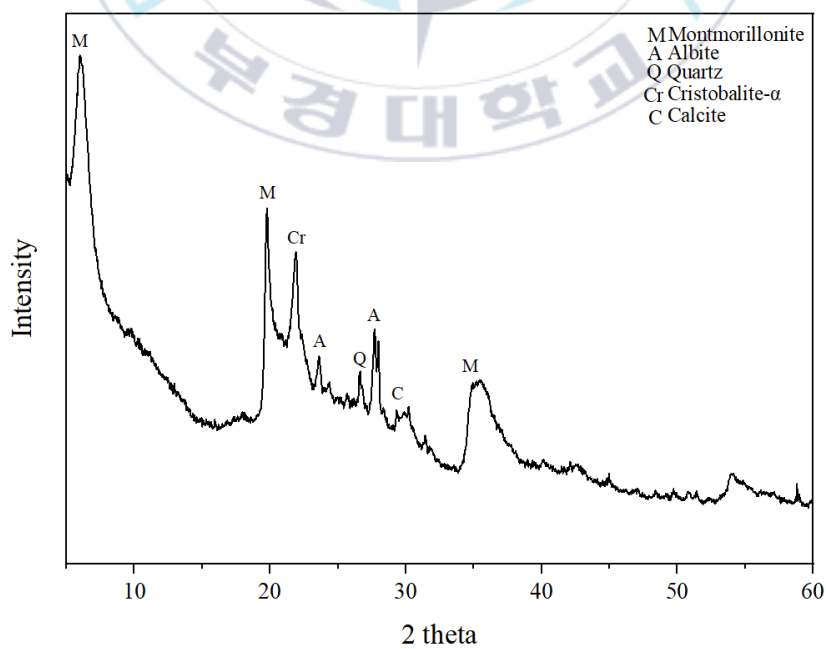


Fig. 10. Result of the XRD analysis of the Bentonil-WRK

#### 4.1.4. Water quality of the groundwater used in the modeling

Data used in the modeling process for the groundwater quality was provided by the KAERI (Korea Atomic Energy Research Institute) for the DB-3 location sample at the KURT (KAERI Underground Research Tunnel). The data were employed as the initial conditions for groundwater in this modeling. Groundwater from DB-3 location was sampled at a depth of 500 meters and found to be reductive groundwater with an Eh value of -436 mV. Furthermore, the groundwater was classified as the Na-Cl type groundwater, indicating relatively high concentrations of Na<sup>+</sup> and Cl<sup>-</sup> (Table 3). In order to perform the geochemical reaction modeling, the Eh value was converted to the pe value, and the ion concentration unit was converted to the molar concentration. The conversion from Eh value to pe value was converted using the Nernst equation (eq.8).

$$Eh = E^0 + \frac{RT}{nF} \ln \left( \frac{Red}{Oxi} \right) \quad (8)$$

where,  $Eh$  is the oxidation potential,  $E^0$  is the standard potential,  $R$  is the ideal gas constant ( $8.314 \text{ J}\cdot\text{K}^{-1}\cdot\text{mol}^{-1}$ ),  $T$  is the temperature in Kelvins,  $n$  is the number of electrons,  $F$  is the faraday constant ( $96,485.332 \text{ C}\cdot\text{mol}^{-1}$ ),  $Red$  is the activity of the reduced form and  $Oxi$  is the activity of the oxidized form. The activity of the electron (pe) is a function of the activity of the reduced and oxidized forms. Therefore, the Eh values were converted to pe values using the following equation (eq. 9)

$$Eh = \frac{2.303RT}{F} pe \quad (9)$$

Table 3. Characteristics of groundwater sample at DB-3 site in the KURT (KAERI).

<b>KURT groundwater</b>	
<b>Chemical composition</b>	
Temp (°C)	14.8
pH	9.05
Eh (mV)	-438
pe	-7.67
<b>Component</b>	<b>Concentration (Moles)</b>
Na <sup>+</sup>	1.65E-03
Ca <sup>2+</sup>	1.43E-04
K <sup>+</sup>	8.46E-06
Mg <sup>2+</sup>	1.20E-05
SiO <sub>2</sub>	1.25E-04
HCO <sub>3</sub> <sup>-</sup>	1.30E-03
Cl <sup>-</sup>	1.47E-03
SO <sub>4</sub> <sup>2-</sup>	6.05E-05
NO <sub>3</sub> <sup>-</sup>	1.10E-05
F <sup>-</sup>	4.27E-04
Al	2.73E-06
Fe	1.24E-07
Sr	2.66E-06
U	6.34E-09

#### 4.1.5. Gas phase interaction in the model

In the initial stage of SNF repository construction, atmospheric gases exist in pore spaces of the multi-barrier as well as in the cavity, and the atmospheric pressure is maintained at 1 atm. The partial pressure of the atmospheric gases remaining in the buffer zone is 0.79 atm of N<sub>2</sub> gas, 0.2 atm of O<sub>2</sub> gas and 0.0004 atm of CO<sub>2</sub> gas in the model. The inflow of groundwater will gradually increase the pore pressure, resulting in the increased partial pressure of the atmospheric constituent gases in the pore. Although the Henry's law, with the assumption of an ideal gas, is commonly used to characterize the behavior of gases, it is more appropriate to consider the behavioral equations of a non-ideal gas, which address the interaction of gases and liquids in high-pressure and high-temperature environments, where the pore pressure is increased to 5 MPa by the inflow of groundwater. Accordingly, the equilibrium between gas and groundwater, representing the initial condition for this model was applied with assuming the behavior of a non-ideal gas under high pressure using the Peng-Robinson equation of state (eq. 10) (Peng & Robinson, 1976). This equation predicts the state of the gas under high pressure condition and considers the gas molecular interactions and the interaction between gas and liquid in high pressure and high temperature environments more accurately. Additionally, it can reflect the solubility and the reactivity of gas in groundwater.

$$P = \frac{RT}{V_m} - \frac{a\alpha}{V_m^2 + 2bV_m + b^2} \quad (10)$$

where,  $P$  is the pressure,  $R$  is the ideal gas constant (8.314 J·K<sup>-1</sup>·mol<sup>-1</sup>),  $T$  is the temperature in Kelvins,  $V_m$  is the volume,  $a$  is the attraction parameter,  $b$  is the repulsion parameter and  $\alpha$  is the temperature-dependent function in the equation.

#### 4.1.6 Microbial activity in the modeling

The microbial activity can affect the geochemical reactions occurred in the buffer zone as well as dissolution and precipitation of minerals in bentonite. The microbial respiration reactions for organic matter degradation in the buffer zone were considered to result in the changes in redox transitions and the additional generation of reactive gases due to the evolution of the hydrogeological environment of the SNF repository. Model studies on the property changes of the buffer material due to microbial activity at the redox repository environment were performed and several assumptions for the microbial activity were applied for this model study.

1. The electron acceptors affecting the microbial growth rate were limited to  $O_{2(aq)}$  and  $SO_4^{2-(aq)}$ , and the organic matter available for oxidation was assumed to be represented as  $CH_2O$ .
2. The depletion rate of electron acceptors in the system was assumed to reach a steady state, where microbial growth and mortality were balanced.
3. It was considered that sufficient microorganisms to degrade organic matter exist and the microbial respiration was not limited by the concentration of organic matter.

The degradation of organic matter in the buffer zone by the microbial activity was designed by using the basic form of the Monod equation (eq. 11).

$$R = k_{max} \frac{[C]}{K_R + [C]} \quad (11)$$

where,  $R$  is the growth rate ( $\text{mol}\cdot\text{m}^{-3}\cdot\text{sec}^{-1}$ ),  $k_{max}$  is the maximum growth rate ( $\text{mol}\cdot\text{m}^{-3}\cdot\text{sec}^{-1}$ ),  $K_R$  is the half-saturation constant ( $\text{mol}\cdot\text{L}^{-1}$ ) and  $[C]$  is the concentration of the limiting substrat S ( $\text{mol}\cdot\text{L}^{-1}$ ). Reaction equations used for the

degradation of organic matter considered in this modeling are shown in Table 4. Reactions were considered in both aerobic and anaerobic environments. The parameters used in the reaction equations are also shown in Table 5.

Table 4. Reaction equations for microbial decomposition of organic matter used in the modeling.

Reaction matter	Electron acceptor	Reaction equation	
CH <sub>2</sub> O	O <sub>2(aq)</sub>	CH <sub>2</sub> O <sub>(aq)</sub> + O <sub>2(aq)</sub> = CO <sub>2(aq)</sub> + H <sub>2</sub> O <sub>(aq)</sub>	Aerobic condition
	SO <sub>4</sub> <sup>2-</sup> <sub>(aq)</sub>	2CH <sub>2</sub> O <sub>(aq)</sub> + SO <sub>4</sub> <sup>2-</sup> <sub>(aq)</sub> + H <sup>+</sup> <sub>(aq)</sub> = 2CO <sub>2(aq)</sub> + HS <sup>-</sup> <sub>(aq)</sub> + 2H <sub>2</sub> O <sub>(aq)</sub>	Anaerobic condition

Table 5. Parameters for microbial oxidation and reduction kinetics in the modeling.

Symbol	Parameter description	Value (mol·m <sup>-3</sup> ·sec <sup>-1</sup> )
$k_{max1}$	Specific Monod reaction rate of organotrophic oxygen reduction	$4.9 \times 10^{-6*}$
$k_{max2}$	Specific Monod reaction rate of organotrophic sulfate reduction	$9.5 \times 10^{-11§§}$
$K_{O_2}$	Half-saturation concentration for O <sub>2</sub> for organotrophic oxygen reduction	$2.5 \times 10^{-4*}$
$K_{SO_4^{2-}}$	Half-saturation concentration for SO <sub>4</sub> <sup>2-</sup> for organotrophic sulfate reduction	$1.0 \times 10^{-5§}$

\*Puigdomènech et al., (2001). §Nethe-Jaenchaen and Thauer (1984). §§Kiczka et al., (2021).

#### 4.1.7. Mineral dissolution and precipitation in the modeling

The dissolution and precipitation reaction of Bentonil-WRK was simulated over a 100,000-year period using the kinetic reaction modeling at high temperature and pressure conditions. This kinetic reaction process started at the presence of KURT groundwater in equilibrium with the atmosphere and the microbial respiration under both aerobic and anaerobic conditions was also included. For mineral dissolution and precipitation reaction modeling, minerals such as Ca-montmorillonite, albite, cristobalite-alpha, quartz, and calcite were selected as reactive minerals of Bentonil-WRK in this study. Secondary precipitated minerals considered in the modeling were kaolinite, dolomite, chalcedony, and pyrite. Results of the quantitative XRD analysis for the Bentonil-WRK constituent minerals, which were required for the geochemical reaction modeling, are shown in Tabel 6. Even the quantitative XRD analysis of Bentonil-WRK did not support the presence of calcite, trace amounts of carbonate were determined to be present through the laboratory experiment and the geochemical modeling was conducted with 1 wt% calcite. Thermodynamic data for minerals at 60°C used in the modeling are shown in Table 7 and most of them were obtained from the LLNL database. It was expected that modeling results provide quantitative data on long-term changes in mineral composition of the bentonite and show the changes in mineral volume and in the porosity of the bentonite over the 100,000-years reaction period.

Table 6. Results of quantitative XRD analysis (wt%) for mineral constituents in the Bentonil-WRK(Cha et al., 2023).

Mineral	Content (wt%)
Montmorillonite	69.8
Albite	15.0
Cristobalite	13.3
Quartz	1.9

Table 7. Thermodynamic constants of bentonite constituent mineral and secondary mineral used in the modeling at 60°C.

Mineral	Structural formula	Log K (60°C)
Phases observed in Bentonil-WRK		
Montmorillonite-Ca	$\text{Ca}_{0.165}\text{Mg}_{0.33}\text{Al}_{1.67}\text{Si}_4\text{O}_{10}(\text{OH})_2 + 6\text{H}^+ = 0.165\text{Ca}^{2+} + 0.33\text{Mg}^{2+} + 1.67\text{Al}^{3+} + 4\text{H}_2\text{O} + 4\text{SiO}_2$	0.31
Albite	$\text{NaAlSi}_3\text{O}_8 + 4\text{H}^+ = \text{Al}^{3+} + \text{Na}^+ + 2\text{H}_2\text{O} + 3\text{SiO}_2$	1.57
Cristobalite	$\text{SiO}_2 = \text{SiO}_2$	-2.99
Quartz	$\text{SiO}_2 = \text{SiO}_2$	-3.47
Calcite	$\text{CaCO}_3 + \text{H}^+ = \text{Ca}^{2+} + \text{HCO}_3^-$	1.32
Phases tested in precipitation		
Kaolinite	$\text{Al}_2\text{Si}_2\text{O}_5(\text{OH})_4 + 6\text{H}^+ = 2\text{Al}^{3+} + 2\text{SiO}_2 + 5\text{H}_2\text{O}$	3.84
Dolomite	$\text{CaMg}(\text{CO}_3)_2 + 2\text{H}^+ = \text{Ca}^{2+} + \text{Mg}^{2+} + 2\text{HCO}_3^-$	1.32
Chalcedony	$\text{SiO}_2 = \text{SiO}_2$	-3.75
Pyrite	$\text{FeS}_2 + \text{H}_2\text{O} = 0.25\text{H}^+ + 0.25\text{SO}_4^{2-} + \text{Fe}^{2+} + 1.75\text{HS}^-$	-22.77

Dissolution and precipitation reaction equations for the Bentonil-WRK constituent minerals in the modeling could be formulated by using equations of the transition state theory of Lasaga (1981, 1984) and Aagaard & Helgeson (1982) (eq. 12).

$$r_m = A_m k(T) (a_{H^+})^n \left[ 1 - \frac{Q_m}{K_m} \right] \quad (12)$$

Where,  $r_m$  is the dissolution and precipitation reaction rate ( $\text{mol}\cdot\text{m}^{-3}\cdot\text{sec}^{-1}$ ),  $A_m$  is the specific surface area ( $\text{m}^2\cdot\text{m}^{-3}$ ),  $k(T)$  is the temperature dependent rate constant ( $\text{mol}\cdot\text{m}^{-2}\cdot\text{sec}^{-1}$ ),  $(a_{H^+})^n$  is the proton activity raised to the power  $n$ ,  $Q_m$  is the ion activity product for this reaction, and  $K_m$  is the equilibrium constant. The temperature dependent rate constant  $k(T)$  was represented by the Arrhenius equation (eq.13). Because the dissolution and precipitation reaction rate of mineral were dependent on the pH, the equation was modified by allaying rate constants specific to acid, neutral and base environments (eq. 14).

$$k(T) = k_{25} \exp \left[ \frac{E_a}{R} \left( \frac{1}{T} - \frac{1}{298.15} \right) \right] \quad (13)$$

Where,  $k_{25}$  is the rate constant at  $25^\circ\text{C}$  ( $\text{mol}\cdot\text{m}^{-2}\cdot\text{sec}^{-1}$ ),  $E_a$  is the activation energy of reaction ( $\text{KJ}\cdot\text{mol}^{-1}$ ),  $R$  is the ideal gas constant ( $8.314 \text{ J}\cdot\text{K}^{-1}\cdot\text{mol}^{-1}$ ), and  $T$  is the absolute temperature (K).

$$r = A_m \left[ k_a \exp \left[ \frac{-E_a}{R} \left( \frac{1}{T} - \frac{1}{298.15} \right) \right] (a_{H^+})^n \left[ 1 - \frac{Q_m}{K_m} \right] + k_n \exp \left[ \frac{-E_a}{R} \left( \frac{1}{T} - \frac{1}{298.15} \right) \right] + k_b \exp \left[ \frac{-E_a}{R} \left( \frac{1}{T} - \frac{1}{298.15} \right) \right] \right] \quad (14)$$

The secondary precipitation minerals were treated with simple reaction equations (eq. 15) due to the lack of data on reaction rates and activation energy as a function of temperature.

$$r_m = A_m k \left[ 1 - \frac{Q_m}{K_m} \right] \quad (15)$$

The kinetic parameters of the Bentonil-WRK component minerals used in the geochemical modeling are shown in Table 8, and the kinetic parameters of the secondary precipitation minerals are shown in Table 9. In dissolution-precipitation reaction modeling of minerals, reaction rates can be significantly influenced by the specific surface area of the minerals. For this modeling, the specific surface area data were referred from the MX-80 Bentonite data from Bildstein et al., 2006.

Table 8. Kinetic reaction modeling parameters of the bentonite minerals applied in this modeling.

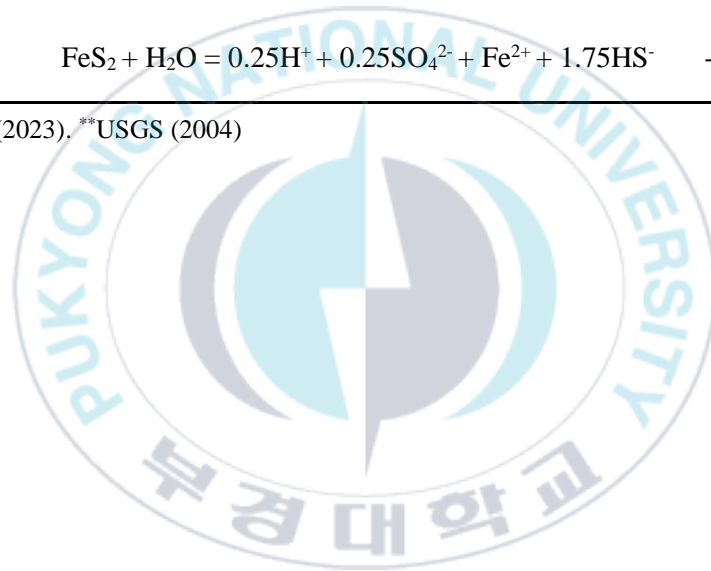
	Acid			Neutral		Base		
	Log $k$ (mol·m <sup>-2</sup> ·s <sup>-1</sup> )	E <sub>a</sub> (KJ·mol <sup>-1</sup> )	n	Log $k$ (mol/m <sup>2</sup> /s)	E <sub>a</sub> (KJ·mol <sup>-1</sup> )	Log $k$ (mol·m <sup>-2</sup> ·s <sup>-1</sup> )	E <sub>a</sub> (KJ·mol <sup>-1</sup> )	n
Montmorillonite*	-12.71	48.00	0.22	-14.41	48.00	-14.41	48.00	-0.13
Albite*	-10.16	65.00	0.46	-12.56	69.80	-15.60	71.00	-0.57
Cristobalite*	-	-	-	-12.31	65.00	-	-	-
Quartz*	-	-	-	13.40	90.90	-	-	-
Calcite*	-0.30	14.40	1.00	-5.81	23.50	-3.48	35.40	1.00

\*USGS (2004).

Table 9. Kinetic reaction modeling parameters of the secondary precipitation minerals applied in this modeling.

Secondary mineral	Structural formula	Log $k$ (mol·m <sup>-2</sup> ·s <sup>-1</sup> )
Kaolinite	$\text{Al}_2\text{Si}_2\text{O}_5(\text{OH})_4 + 6\text{H}^+ = 2\text{Al}^{3+} + 2\text{SiO}_2 + 5\text{H}_2\text{O}$	-14.00*
Dolomite	$\text{CaMg}(\text{CO}_3)_2 + 2\text{H}^+ = \text{Ca}^{2+} + \text{Mg}^{2+} + 2\text{HCO}_3^-$	-10.00*
Chalcedony	$\text{SiO}_2 = \text{SiO}_2$	-14.50**
Pyrite	$\text{FeS}_2 + \text{H}_2\text{O} = 0.25\text{H}^+ + 0.25\text{SO}_4^{2-} + \text{Fe}^{2+} + 1.75\text{HS}^-$	-4.55**

\*Sin et al., (2023). \*\*USGS (2004)



## CHAPTER 5. RESULTS AND DISCUSSION

### 5.1. Equilibrium geochemical reaction modeling

#### 5.1.1. Change of KURT groundwater quality at the equilibrium reaction modeling with atmospheric gases

Results for the reaction modeling between the KURT groundwater and the atmospheric gases at equilibrium condition are shown in Table 10 and Table 11. From water quality data, the initial KURT groundwater was originated from the reduced condition (shown in Table 3). As the KURT groundwater starts to react with O<sub>2</sub> gas and CO<sub>2</sub> gas, the groundwater quality was changed to be exposed to an aerobic environment. The pH and the pe of groundwater changed to 4.6 and 14.1, respectively, supporting that the initially reducing environment of the KURT groundwater has been changed to an aerobic environment (Table 10). It comes from the fact that CO<sub>2</sub> and O<sub>2</sub> gases from the atmospheric constituents have dissolved into the groundwater. Under high pressure condition of 5 MPa, the solubility of gases in groundwater was increased and more gases existed as dissolved phases (or ions) in groundwater, promoting geochemical reactions. The gas volume also decreased from the initial 1 L to 6.13E-03 L, and the partial pressures of the atmospheric constituent gases increased (N<sub>2</sub> gas to 44.9 atm, CO<sub>2</sub> gas to 0.087 atm, and O<sub>2</sub> gas to 5 atm) (Table 11). In reaction equilibrium at high temperature (60°C) and pressure (5 MPa) conditions, the concentration of HCO<sub>3</sub><sup>-</sup>, CO<sub>2(aq)</sub>, and O<sub>2(aq)</sub> were 2.60E-05E mol/L, 1.27E-03E mol/L, 4.20E-03 mol/L, respectively in the modeling.

Table 10. Adjusted KURT groundwater quality after the geochemical reaction modeling.

<b>KURT groundwater</b>	
<b>Chemical composition</b>	
Temp (°C)	60.0
Pressure (atm)	50.0
pH	4.6
pe	14.1
<b>Component</b>	<b>Concentration (Moles)</b>
Na <sup>+</sup>	1.65E-03
Ca <sup>2+</sup>	1.41E-04
K <sup>+</sup>	8.45E-06
Mg <sup>2+</sup>	1.15E-05
SiO <sub>2(aq)</sub>	1.25E-04
HCO <sub>3</sub> <sup>-</sup>	2.60E-05
CO <sub>2(aq)</sub>	1.27E-03
O <sub>2(aq)</sub>	4.20E-03
Cl <sup>-</sup>	1.47E-03
SO <sub>4</sub> <sup>2-</sup>	5.82E-05
NO <sub>3</sub> <sup>-</sup>	1.10E-05
F <sup>-</sup>	4.27E-04
Al	2.73E-06
Fe	1.24E-07
Sr	2.66E-06
U	6.34E-09



Table 11. Changes in the partial pressure of atmospheric gases after initial KURT groundwater-Atmosphere equilibrium modeling.

	Partial pressure (atm)			Total gas volume (L)	Total gas pressure (atm)
	pN <sub>2</sub>	pCO <sub>2</sub>	pO <sub>2</sub>		
Initial stage	0.79	0.0004	0.2	1	1
Equilibrium stage	44.9	0.087	5	0.00613	50

## 5.2. Kinetic geochemical reaction modeling

### 5.2.1. Change of the KURT groundwater composition over the reaction time

Kinetic geochemical reaction modeling was conducted to investigate the temporal changes in KURT groundwater quality by the further geochemical reaction. As shown in Fig. 10, the pH of KURT groundwater initially decreased to 4.6 due to the dissolution of atmospheric gases and to the increase in temperature. However, it was buffered through interactions with bentonite and the dissolution of calcite, resulting in a gradual rise of the pH to 6.36 after 100,000 years (Fig. 11). Changes in the pe of groundwater supported that it initially increased to 14.1 due to the presence of atmospheric O<sub>2</sub>, creating an aerobic environment. However, after approximately 5,190 years, the pe transitions to negative values occurred, indicating a shift to an anaerobic environment by the microbial activity and the O<sub>2</sub> consumption (Fig. 11). These modeling results indicated that, after 5,190 years, oxygen in the KURT groundwater was completely consumed.

Modeling results for changes in oxygen ion and sulfur ion concentrations in KURT groundwater showed that the oxygen ion concentration decreased very rapidly in the initial reaction stage, indicating that in the early oxygen-rich environment, the activity of aerobic microorganisms was vigorous, resulting in rapid oxygen consumption. After about 60 years, the oxygen concentration decreased to  $1.00\text{E-}6$  mol, and it is observed that the oxygen in groundwater was completely depleted after 5,190 years (Fig. 12 (a)). The geochemical reaction modeling performed in this study considered only aerobic microbial respiration among the various oxygen-consuming mechanisms occurred in the SNF repository. Corrosion of copper canisters and oxidation of sulfide minerals will be included as additional geochemical reactions as well as microbial activity as the further study. From the modeling results, the sulfur concentration in groundwater indicated that after the complete depletion of oxygen (after 5,190 years), the sulfate is reduced, leading to the formation of bisulfide (Fig. 12 (b)).

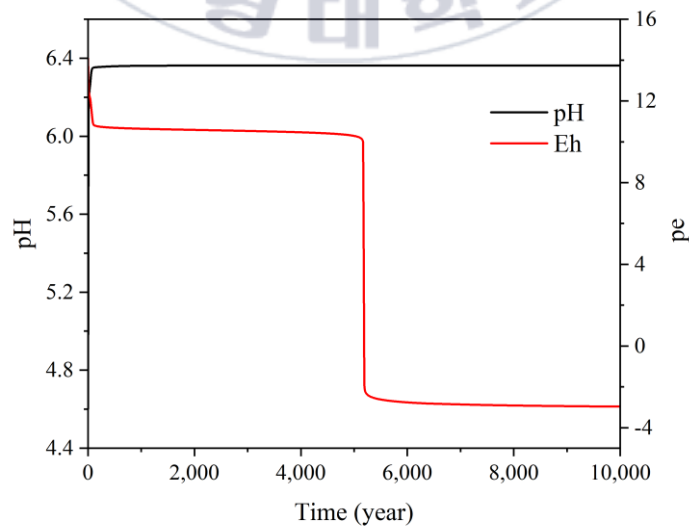


Fig. 11. Modeling results of KURT groundwater pH and pe changes over 10,000 years.

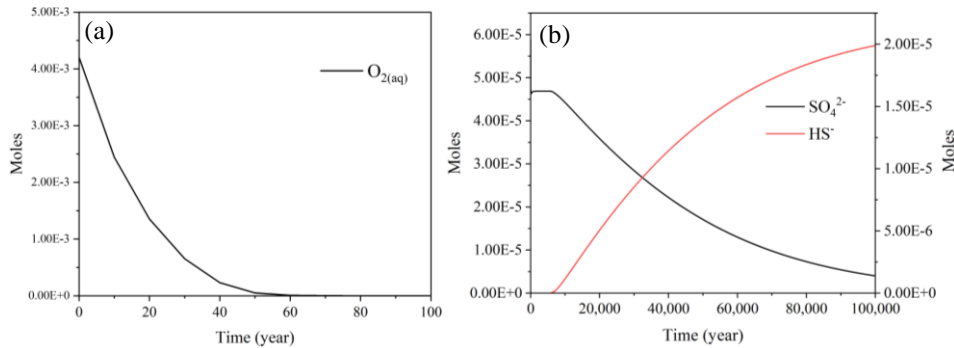


Fig. 12. Results of changes in the initial groundwater oxygen concentration (a) and the sulfur concentration (b).

### 5.2.2. Change of the gas concentration over reaction time

A kinetic geochemical reaction modeling results showed that the temporal changes of gas concentrations in groundwater over the reaction time (Fig. 13). By the equilibrium reaction process between the gas phase and the KURT groundwater, the initially present atmospheric  $O_2$  gas was continuously dissolved into the KURT groundwater and dissolved  $O_2$  was consumed by the aerobic microbial respiration. It was also observed that  $CO_2$  gas was continuously produced due to oxygen consumption during the microbial respiration. In addition, as shown in Fig. 14,  $H_2S$  gas was generated during the process where all oxygen was consumed, and sulfate was reduced to bisulfide (Fig. 14). As the gases were generated and dissolved, changes both in gas partial pressures occurred. Table 12 shows the partial pressures of the gases over time and shows that the  $H_2S$  gas was produced after the  $O_2$  gas was completely consumed (Table 12).

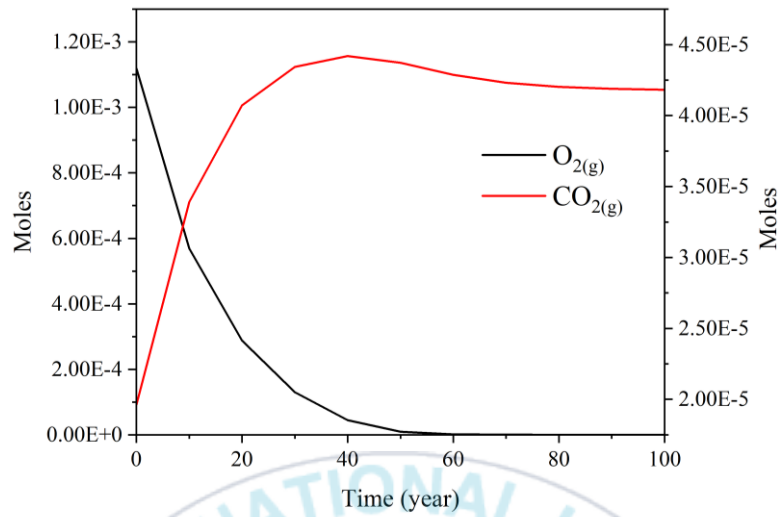


Fig. 13. Results of changes in the concentration of atmospheric gases.

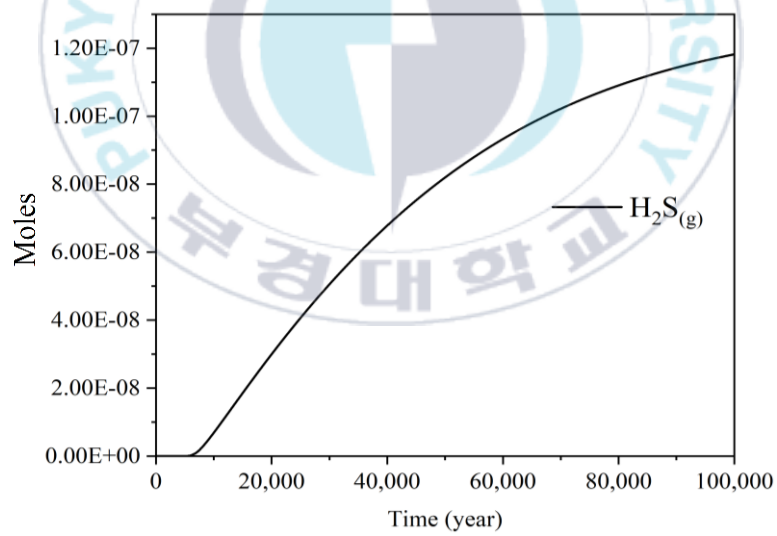
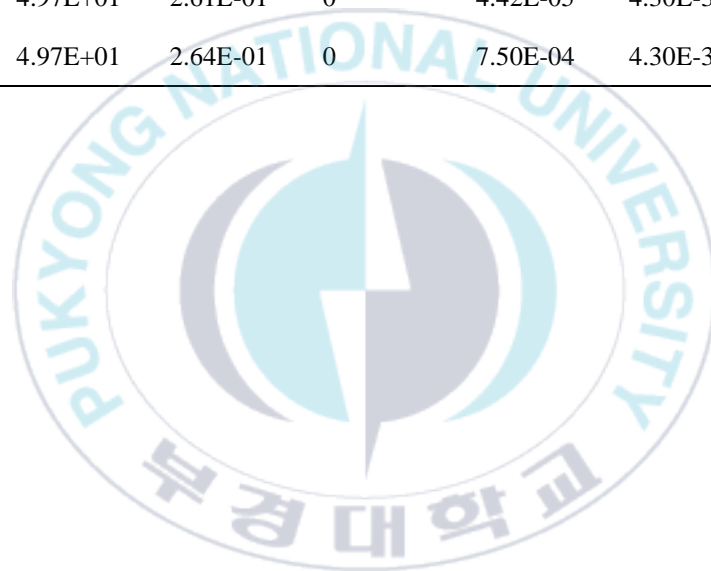


Fig. 14. Results of modeling for the concentration changes of the generated  $H_2S$  gas.

Table 12. Results of changes in atmospheric partial pressure over 100,000 years.

Time (year)	Partial pressure (atm)				Total gas volume (L)
	pN <sub>2</sub>	pCO <sub>2</sub>	pO <sub>2</sub>	pH <sub>2</sub> S	
0	4.49E+1	8.70E-02	5.00E-00	0	1
500	4.97E+01	2.63E-01	1.37E-06	0	4.30E-3
1,000	4.97E+01	2.62E-01	9.19E-07	0	4.30E-3
5,000	4.97E+01	2.61E-01	3.74E-08	0	4.30E-3
10,000	4.97E+01	2.61E-01	0	4.42E-05	4.30E-3
100,000	4.97E+01	2.64E-01	0	7.50E-04	4.30E-3



### 5.2.3. Change of the mineral composition in bentonite over the reaction time

A kinetic geochemical reaction modeling study for the temporal changes in the amount of the bentonite constituent minerals and the precipitated minerals was conducted and its results were presented over a total reaction period of 100,000 years. Fig. 15 and Fig. 16 showed the quantitative modeling results for montmorillonite and for calcite, respectively. Both montmorillonite and calcite showed rapid dissolution in the initial stages, followed by a decrease in dissolution rate as they reach chemical equilibrium. Most of bentonite minerals such as montmorillonite and calcite dissolved actively at low pH conditions. Equilibration with the initial atmospheric gases led to the formation of low pH groundwater, which accelerated the dissolution rates of montmorillonite and calcite. However, as the pH was buffered closer to the neutral, the dissolution rates of minerals became to decrease. Montmorillonite showed a mass loss of 0.0021% after 100,000 years (Fig. 15), and the mass of calcite also decreased by 0.37% after 100,000 years (Fig. 16), suggesting that these quantitative changes are small but clear for the mineral dissolution process. Quartz is one of the very stable minerals, and its dissolution hardly ever happened during the modeling period. Albite and cristobalite were dissolved in such small amounts that they had virtually no effect on the overall mass change of the bentonite, so modeling results produced no tangible mass change of them.

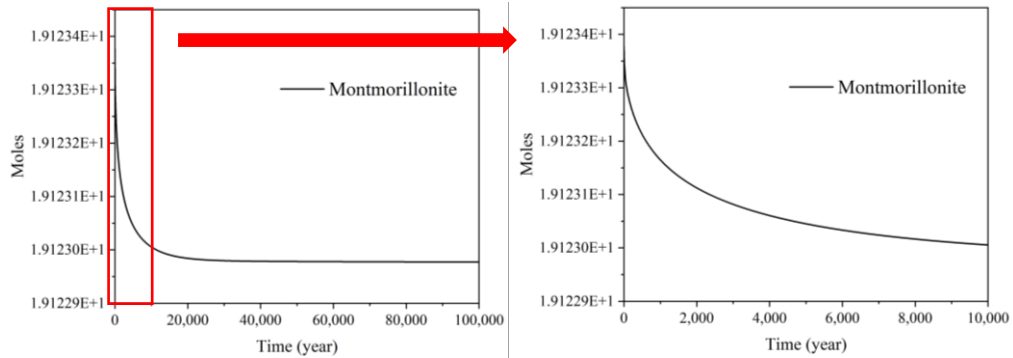


Fig. 15. Results of modeling for the mass changes of montmorillonite in bentonite over 100,000 reaction years (Right: 10,000 years).

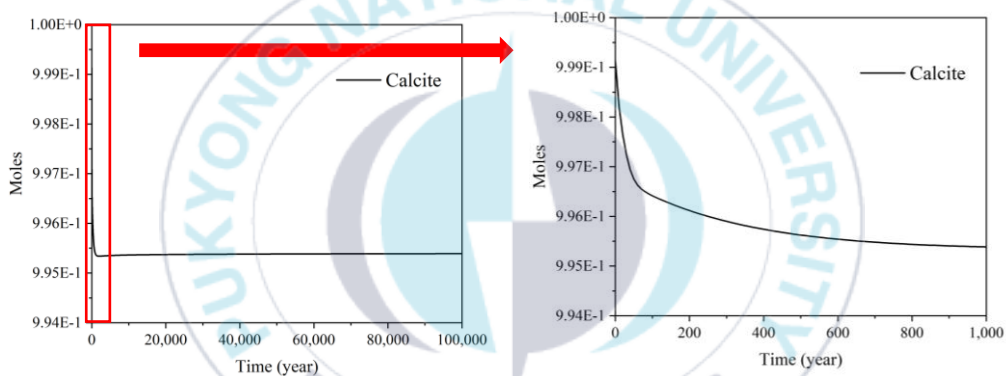
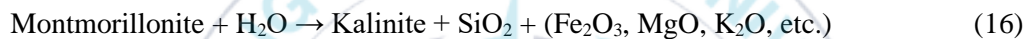


Fig. 16. Results of modeling for the mass change of calcite in bentonite over 100,000 reaction years (Right: 1,000 years).

With the evolution process of the SNF repository environment, it was considered that the dissolution of montmorillonite and calcite, as well as the generation of  $\text{CO}_2$  and  $\text{HS}^-$  ions, could lead to the formation of secondary precipitated minerals such as kaolinite, dolomite, pyrite and chalcedony. In this model study, the precipitation of secondary minerals occurred and their quantitative changes over reaction time were supported as the modeling results. First, the formation of kaolinite was identified as a result of kaolinization caused by the alteration of montmorillonite in bentonite. Montmorillonite, a smectite group mineral, has a 2:1 layered structure of silicon and aluminum (Si-Al-Si). During the alteration process, the silicate layers at the edges of

the structure peeled off, resulting in the formation of kaolinite with an Al-Si layered structure (Altschuler et al., 1963). In acidic environments, an aluminum formed a sixfold coordination structure having high reactivity, which promoted the formation of Si-O-Al bonds, thereby facilitating the formation of kaolinite (Ryu et al., 2008). Consequently, the influence of low pH also caused the exfoliation of montmorillonite surfaces, inducing the transformation and formation of kaolinite with a 1:1 layered structure. The transformation process from montmorillonite to kaolinite could be presented in Eq. 16, and the modeling results of the quantitative changes in kaolinite over the reaction time are shown in Fig. 17.



As shown in Fig. 17, the kaolinite was precipitated rapidly initially and continued to be precipitated steadily over time. This result could be attributed to the rapid initial dissolution of montmorillonite followed by sustained dissolution reactions over time. In addition, the  $\text{Si}^{4+}$  ions were released into groundwater during the transformation of montmorillonite to kaolinite, existing in a supersaturated state and they could be precipitated in the form of chalcedony, a silicate mineral formed under relatively low temperature conditions (Sawaguchi et al., 2016). Modeling results of the quantitative changes in chalcedony over reaction time were shown in Fig. 18. Based on the modeling results, it was suggested that approximately  $5.27\text{E-}04$  moles of kaolinite and  $9.82\text{E-}07$  moles of chalcedony were precipitated after 100,000 years of the reaction.

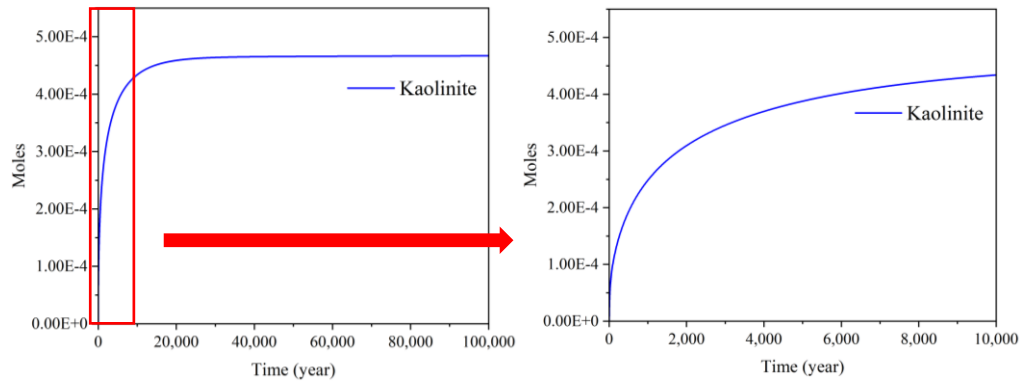


Fig. 17. Results of modeling for the mass change of kaolinite over 100,000 reaction years (Right: 10,000 year).

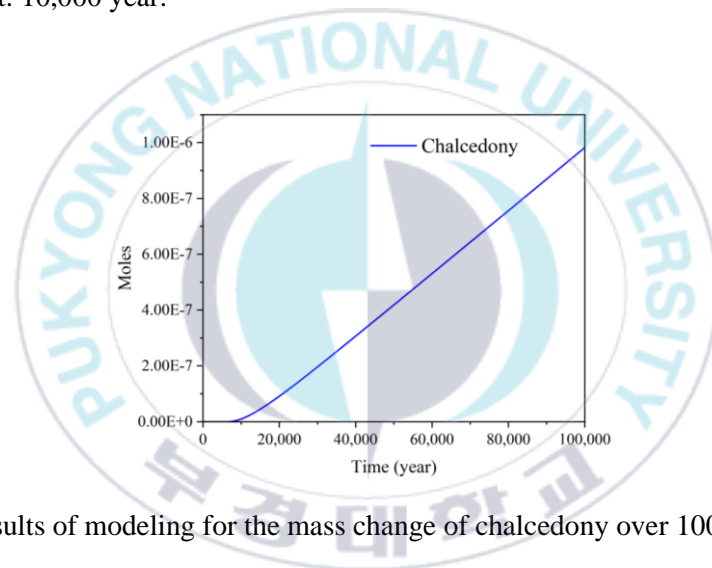


Fig. 18. Results of modeling for the mass change of chalcedony over 100,000 years.

Subsequently, the formation of dolomite was identified as a result of dolomitization caused by alteration of calcite. Calcite is a rhombohedral carbonate mineral of the trigonal system consisting of alternating  $\text{Ca}^{2+}$  and  $\text{CO}_3^{2-}$  ions (Chen et al., 2023). Dolomite can form when  $\text{Ca}^{2+}$  ions in calcite are replaced by  $\text{Mg}^{2+}$  ions. Furthermore, the presence of dissolved carbonate in the system, in addition to the supply of  $\text{Mg}^{2+}$  ions, is essential for dolomite formation (Machel and Mountjoy, 1986). The transformation from calcite to dolomite was shown in Eq. 17, and the modeling results of the quantitative changes in dolomite were shown in Fig. 19.



As shown in Fig. 19, the dolomite was precipitated very rapidly in the early reaction stages. This result is interpreted as being due to the presence of  $\text{Mg}^{2+}$  ions in the KURT groundwater, and the rapid initial dissolution of calcite, and its subsequent reaction with the  $\text{CO}_2$  gas generated. The dissolution of calcite, the generation of  $\text{CO}_2$  gas, and the precipitation of dolomite in the SNF repository environment provided an significant explanation for the mass transition of carbon. Based on the modeling results, it was confirmed that approximately  $6.02\text{E}-04$  moles of dolomite were precipitated after 100,000 years.

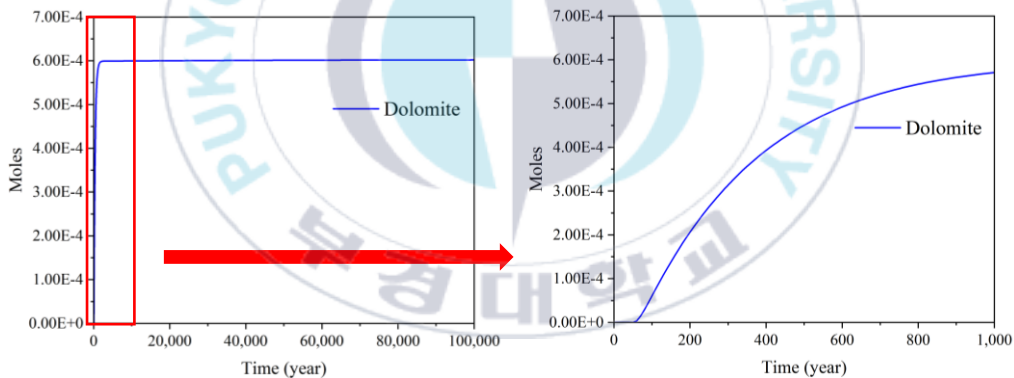


Fig. 19. Results of modeling for the mass change of dolomite over 100,000 years (Right: 1,000 year).

Finally, the formation of pyrite was observed as a result of the  $\text{HS}^-$  ions originated by the reduction of  $\text{SO}_4^{2-}$  ions after complete consumption of oxygen. When the  $\text{HS}^-$  ions were produced by the respiration of sulfate-reducing bacteria existing in a supersaturated state in the system, they combine with the  $\text{Fe}^{2+}$  ions and were precipitated as pyrite, the most stable sulfide mineral. The quantitative changes in pyrite over the reaction time were shown in Fig. 20. From modeling results, pyrite

precipitation began approximately 6,420 years after  $\text{HS}^-$  ions reached a supersaturated state following complete oxygen depletion. It was also observed that pyrite precipitated very rapidly during the initial stages, supporting that the transition from an aerobic to an anaerobic environment in the buffer zone of the SNF repository facilitated the precipitation of pyrite, a sulfide mineral. Based on the modeling results,  $1.24\text{E-}07$  moles of pyrite were precipitated after 100,000 years.

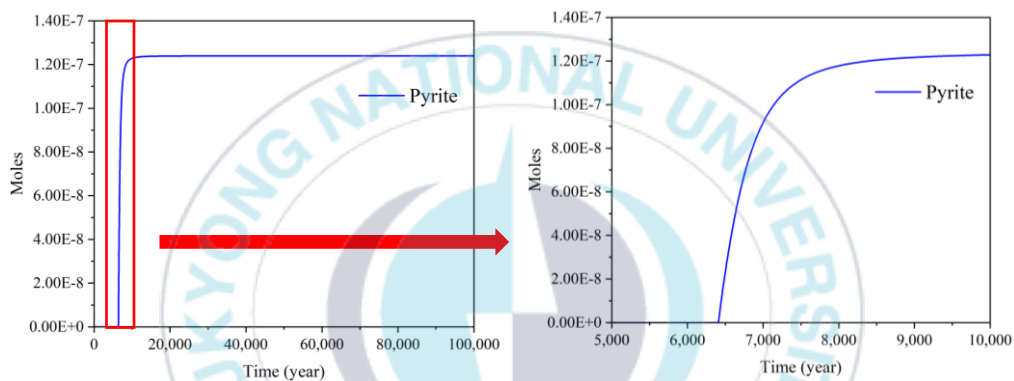
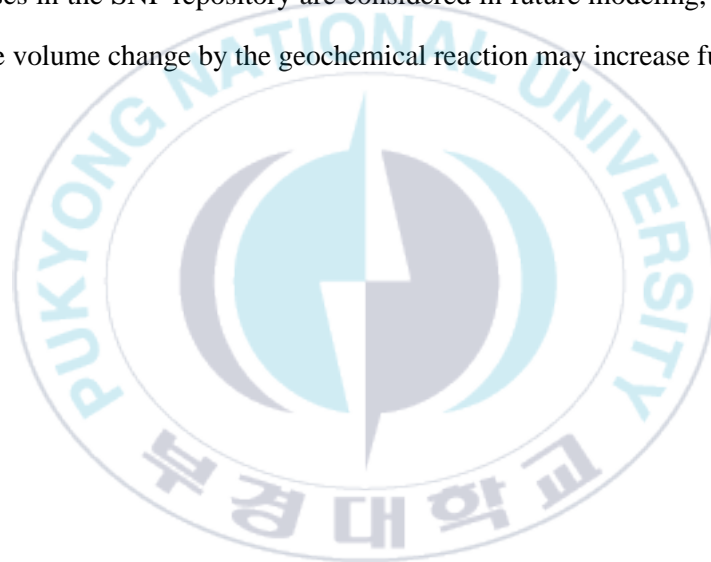


Fig. 20. Results of modeling for the mass change of pyrite over 100,000 years (Right: 10,000 years).

#### 5.2.3.1. Property changes of the Bentonil-WRK over the reaction time

Molar mass change of dissolved or precipitated minerals, and variations in mineral volumes and pore volumes due to geochemical reactions, are shown in Fig. 21. Because the porosity of saturated Bentonil-WRK, which is being considered as a buffer material for the Korean SNF repository, has not been clearly identified, a porosity value of 0.4, as used in previous modeling studies, was assumed to calculate the results for pore volume and mineral volume change (Marty et al., 2010; Fernandez et al., 2009; Watson et al., 2009). As shown in Fig. 21, after 100,000 years of geochemical reaction, the mineral volume decreased by 0.0029%, while the pore volume increased by 0.0043%.

Reduction in mineral volume due to the mass loss in Bentonil-WRK led to an increase in pore volume. Additionally, the generated reactive gases could affect to maintain a relatively acidic environment, resulting in dissolution reactions being dominant over precipitation reactions, although the volume change was confirmed to be minimal. This finding is attributed to the geochemical reaction modeling in this study, being limited to reactive gases such as CO<sub>2</sub> and H<sub>2</sub>S, and considering only a portion of the microbial respiration processes. Therefore, if additional mechanisms for the generation of CO<sub>2</sub> and H<sub>2</sub>S gases in the SNF repository are considered in future modeling, it is expected that the pore volume change by the geochemical reaction may increase further.



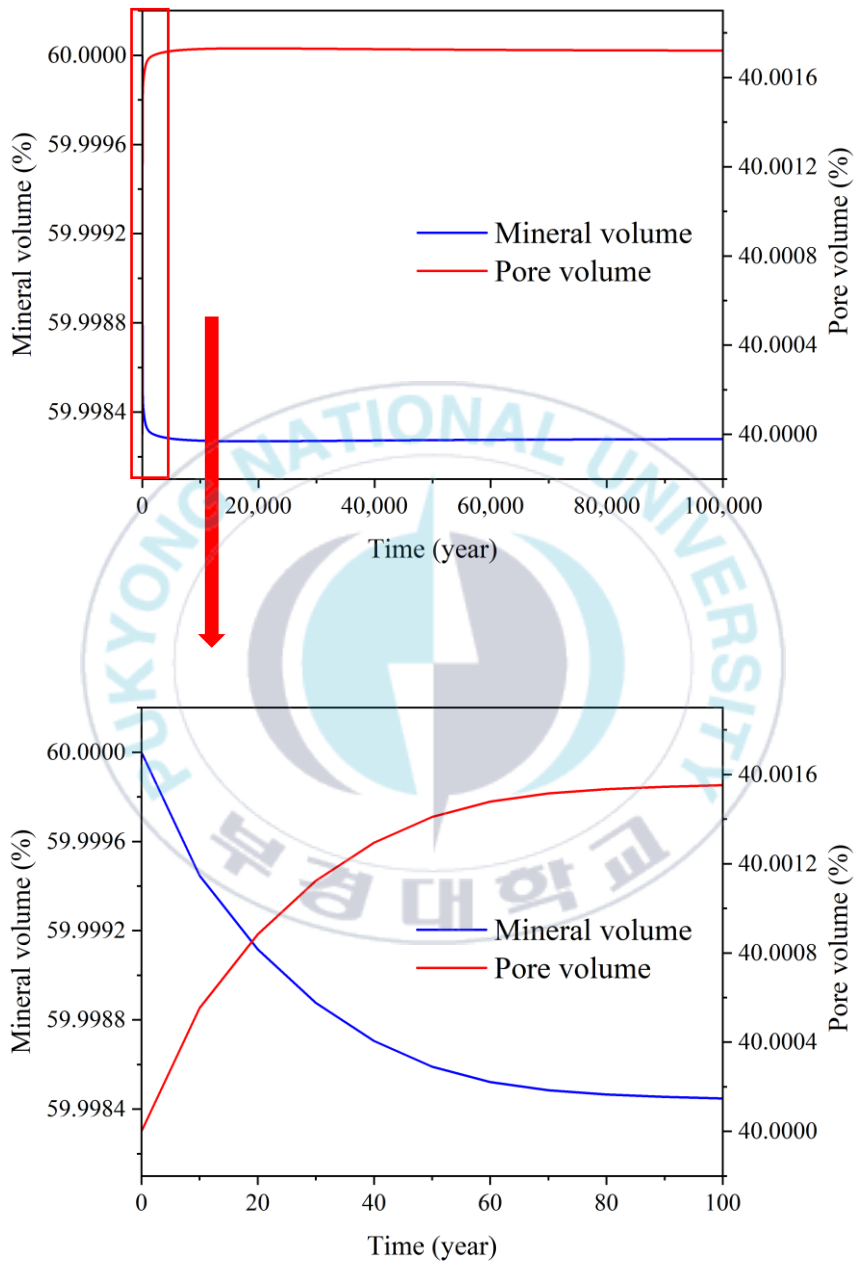


Fig. 21. Results of modeling for the change in bentonite properties over 100,000 years (Bottom: 100 years).

## CHAPTER 6. CONCLUSIONS

This study focused on investigating the effects of reactive gases on the property changes of bentonite (Bentonil-WRK), through the geochemical reaction modeling in the reactive gas-groundwater-bentonite system. The long-term effects of reactive gases, in particular CO<sub>2</sub> and H<sub>2</sub>S, on the properties of Bentonil-WRK were simulated using the geochemical reaction modeling over a period of 100,00 years. For the model study, the geochemical reactions occurred in the buffer zone were divided into three reaction stages; ① equilibrium stage representing the atmospheric gas-groundwater reaction in the pore spaces of the buffer zone, ② the aerobic reaction stage considering the aerobic microbial respiration with O<sub>2</sub> and CO<sub>2</sub> gas and mineral dissolution/precipitation, and ③ the anaerobic reaction stage considering the sulfate reduction and mineral dissolution/precipitation.

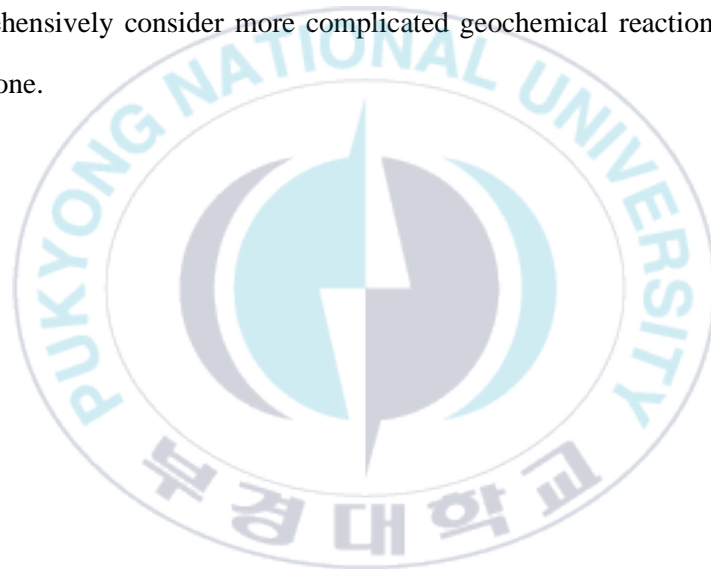
At first, the geochemical reaction between atmospheric gas and KURT groundwater in pore spaces of the buffer zone was simulated at equilibrium reaction condition. Reaction scenarios were designed to account for the dissolution/precipitation reactions of Bentonil-WRK in redox environments and for microbial respiration in the reactive gas-groundwater-bentonite system. Modeling results showed that the inflow of groundwater led to the dissolution of residual atmospheric gases such as CO<sub>2</sub> and O<sub>2</sub>, causing the groundwater quality to transition into an aerobic and low-pH environment. The swelling of bentonite by water saturation increased the pore pressure (5 MPa) of the buffer zone, which increased the CO<sub>2</sub> gas solubility, resulting in the pH decrease to 4.6 at equilibrium between atmospheric gas and KURT groundwater. Aerobic microbial respiration began and constantly consumed O<sub>2</sub> and SO<sub>4</sub><sup>2-</sup> ions, generating

additional CO<sub>2</sub> and H<sub>2</sub>S gases. The complete O<sub>2</sub> consumption occurred after approximately 5,190 years of reaction time. Mineral kinetic modeling results supported that montmorillonite and calcite, as primary minerals in Bentonil-WRK, underwent rapid dissolution in the early stages due to the low pH, showing mass losses of 0.024% and 0.37%, respectively. The precipitation of secondary minerals, including kaolinite, dolomite, chalcedony, and pyrite also occurred as well as the dissolution. The alteration of montmorillonite to kaolinite was investigated in the modeling as a transformation in which the Si layer at the edges of the Si-Al-Si 2:1 layered structure of montmorillonite delaminated, forming a kaolinite having a 1:1 layered structure. Dissolved Si<sup>2+</sup> ions in groundwater became supersaturated and precipitated as chalcedony due to relatively low temperature condition. Dolomite was also found to precipitate as a result of calcite dissolution and the continuous generation of CO<sub>2</sub> gas, reacting with Mg<sup>2+</sup> ions that were present in KURT groundwater. Pyrite as a secondary mineral was also observed to be originated from HS<sup>-</sup> ions, which were generated under the anaerobic conditions by the geochemical reaction, as they precipitated with Fe<sup>2+</sup> ions. These results suggest that the microbial respiration considered in this study could have an effect on the property changes of the buffer material.

From the modeling results over 100,000 reaction time, volume changes of mineral and pore in Bentonil-WRK were observed. Total mineral volume decreased by 0.0029% and pore volume increased by 0.0043% by geochemical reactions in this model study. Even these property changes looked somewhat trivial, but it was quite clear that reactive gases (CO<sub>2</sub>, O<sub>2</sub> and H<sub>2</sub>S) promote geochemical reactions, controlling the behavior of leaked radionuclide in the buffer zone. The geochemical reaction modeling conducted in this study considered only the microbial respiration as the sole mechanism for gas generation. If additional reactive gas generation processes are considered,

property changes of the buffer material could more significantly impact the long-term stability of the buffer in the SNF repository.

Results in this study would support important and quantitative data for the future modeling study including many different reactive gas reaction processes and additional radioactive nuclide reaction mechanisms that may occur in SNF repository environments. They could also serve meaningful data for the long-term stability assessment of the SNF repository and can be extended to advanced modeling studies that comprehensively consider more complicated geochemical reactions occurred in the buffer zone.



## REFERENCES

- Aagaard, P., & Helgeson, H. C. (1982). Thermodynamic and kinetic constraints on reaction rates among minerals and aqueous solutions; I, Theoretical considerations. *American journal of Science*, 282(3), 237-285.
- AB, S. K. (2010). Design and production of the KBS-3 repository. In *SKB Technical Report TR-10-12*. Svensk Kärnbränslehantering AB Stockholm, Sweden.
- AC03659171, A. (Ed.). (2003). *Scientific and technical basis for the geological disposal of radioactive wastes*. Internat. Atomic Energy Agency.
- Acero, P., Auqué, L. F., Gimeno, M. J., & Gómez, J. B. (2010). Evaluation of mineral precipitation potential in a spent nuclear fuel repository. *Environmental Earth Sciences*, 59, 1613-1628.
- Altschuler, Z. S., Dwornik, E. J., & Kramer, H. (1963). Transformation of montmorillonite to kaolinite during weathering. *Science*, 141(3576), 148-152.
- Bagnoud, A., Chourey, K., Hettich, R. L., De Bruijn, I., Andersson, A. F., Leupin, O. X., Schwyn, B., & Bernier-Latmani, R. (2016). Reconstructing a hydrogen-driven microbial metabolic network in Opalinus Clay rock. *Nature communications*, 7(1), 12770.
- Bildstein, O., Trotignon, L., Perronnet, M., & Jullien, M. (2006). Modelling iron–clay interactions in deep geological disposal conditions. *Physics and Chemistry of the Earth, Parts A/B/C*, 31(10-14), 618-625.
- Bildstein, O., & Claret, F. (2015). Stability of clay barriers under chemical perturbations. In *Developments in Clay Science* (Vol. 6, pp. 155-188). Elsevier.

- Bond, A. E., Hoch, A. R., Jones, G. D., Tomczyk, A. J., Wiggin, R. M., & Worraker, W. J. (1997). Assessment of a spent fuel disposal canister. Assessment studies for a copper canister with cast steel inner component.
- Bruckner, T., Fulton, L., Hertwich, E., McKinnon, A., Perczyk, D., Roy, J., Schaeffer, R., Schlömer, S., Sims, R., Smith, P., & Wisser, R. (2014). Technology-specific cost and performance parameters [annex III]. In *Climate change 2014: mitigation of climate change* (pp. 1329-1356). Cambridge University Press.
- Cha, Y., Lee, C., Kim, J. S., & Lee, M. (2023). Evaluation of thermal-hydro-mechanical behavior of bentonite buffer under heating-hydration condition at disposal hole. *Journal of Korean Tunnelling and Underground Space Association*, 25(2), 175-186.
- Chen, C., Zhong, H., Wang, X., Ning, M., Wang, X., Ge, Y., Wang, H., Tang, R., & Hou, M. (2023). Thermodynamic and Kinetic Studies of Dolomite Formation: A Review. *Minerals*, 13(12), 1479.
- Deng, D., Zhang, L., Dong, M., Samuel, R. E., Ofori-Boadu, A., & Lamssali, M. (2020). Radioactive waste: A review. *Water Environment Research*, 92(10), 1818-1825.
- Ember (2024); Energy Institute - Statistical Review of World Energy (2024) – with major processing by Our World in Data. “Electricity generation from nuclear – Ember and Energy Institute” [dataset]. Ember, “Yearly Electricity Data”; Energy Institute, “Statistical Review of World Energy” [original data].
- Fernandez, R., Cuevas, J., & Mäder, U. K. (2009). Modelling concrete interaction with a bentonite barrier. *European Journal of Mineralogy*, 21(1), 177-191.
- Fernández, R., Ruiz, A. I., & Cuevas, J. (2014). The role of smectite composition on the hyperalkaline alteration of bentonite. *Applied clay science*, 95, 83-94.

- Hung, C. C., Briggs, S., Yu, Y. C., Wu, Y. C., & King, F. (2023). Reactive-transport model for the production, transport, and consumption of sulfide in a spent nuclear fuel deep geological repository in crystalline rock. *Materials and Corrosion*, 74(11-12), 1848-1860.
- IAEA (International Atomic Energy Agency), 1994, Classification of Radioactive Waste: A Safety Guide.
- Itäla, A., Järvinen, J., & Muurinen, A. (2013). CO<sub>2</sub> effect on the pH of compacted bentonite buffer on the laboratory scale. *Clay Minerals*, 48(2), 277-284.
- Jain, D. K., Providenti, M., Tanner, C., Cord, I., & Stroes-Gascoyne, S. (1997). Characterization of microbial communities in deep groundwater from granitic rock. *Canadian journal of microbiology*, 43(3), 272-283.
- Jalique, D. R., Stroes-Gascoyne, S., Hamon, C. J., Priyanto, D. G., Kohle, C., Evenden, W. G., Wolfaardt, G. M., Grigoryan, A. A., Mckelvie, J., & Korber, D. R. (2016). Culturability and diversity of microorganisms recovered from an eight-year old highly-compacted, saturated MX-80 Wyoming bentonite plug. *Applied Clay Science*, 126, 245-250.
- Karland, O. (2010). Chemical and mineralogical characterization of the bentonite buffer for the acceptance control procedure in a KBS-3 repository.
- Kiczka, M., Pekala, M., Maanoja, S., Muuri, E., & Wersin, P. (2021). Modelling of solute transport and microbial activity in diffusion cells simulating a bentonite barrier of a spent nuclear fuel repository. *Applied Clay Science*, 211, 106193.
- Kim, J. S., Lee, S. Y., Lee, S. H., & Kwon, J. S. (2023b). A Review of the Influence of Sulfate and Sulfide on the Deep Geological Disposal of High-level Radioactive Waste. *Economic and Environmental Geology*, 56(4), 421-433.

- Kim, J., Lee, S., Choi, H., Park, H., & Jung, S. P. (2023a). Global radioactive waste disposal trends and prospects. *J Korean Soc Environ Eng*, 45(4), 210-224.
- Kim, K. I., Lee, C., & Kim, J. S. (2021). A numerical study of the performance assessment of coupled thermo-hydro-mechanical (THM) processes in improved Korean reference disposal system (KRS+) for high-level radioactive waste. *Tunnel and Underground Space*, 31(4), 221-242.
- King, F., Kolář, M., Puigdomenech, I., Pitkänen, P., & Lilja, C. (2021). Modeling microbial sulfate reduction and the consequences for corrosion of copper canisters. *Materials and Corrosion*, 72(1-2), 339-347.
- King, F., Lilja, C., & Vähänen, M. (2013). Progress in the understanding of the long-term corrosion behaviour of copper canisters. *Journal of Nuclear Materials*, 438(1-3), 228-237.
- Lasaga, A. C. (1981). Rate laws of chemical reactions. *Rev. Mineral.:(United States)*, 8.
- Lasaga, A. C. (1984). Chemical kinetics of water-rock interactions. *Journal of geophysical research: solid earth*, 89(B6), 4009-4025.
- Lee, C., Cho, W. J., Lee, J., & Kim, G. Y. (2019). Numerical analysis of coupled thermo-hydro-mechanical (THM) behavior at Korean reference disposal system (KRS) using TOUGH2-MP/FLAC3D simulator. *Journal of Nuclear Fuel Cycle and Waste Technology (JNFCWT)*, 17(2), 183-202.
- Lee, C., Lee, J., Park, S., Kwon, S., Cho, W. J., & Kim, G. Y. (2020a). Numerical analysis of coupled thermo-hydro-mechanical behavior in single-and multi-layer repository concepts for high-level radioactive waste disposal. *Tunnelling and Underground Space Technology*, 103, 103452.

- Lee, J., Cho, D., Choi, H., & Choi, J. (2007). Concept of a Korean reference disposal system for spent fuels. *Journal of Nuclear Science and Technology*, 44(12), 1565-1573.
- Lee, J., Kim, I., Ju, H., Choi, H., & Cho, D. (2020b). Proposal of an improved concept design for the deep geological disposal system of spent nuclear fuel in Korea. *Journal of Nuclear Fuel Cycle and Waste Technology (JNFCWT)*, 18(spc), 1-19.
- Machel, H. G., & Mountjoy, E. W. (1986). Chemistry and environments of dolomitization—a reappraisal. *Earth-Science Reviews*, 23(3), 175-222.
- Marty, N. C., Fritz, B., Clément, A., & Michau, N. (2010). Modelling the long term alteration of the engineered bentonite barrier in an underground radioactive waste repository. *Applied Clay Science*, 47(1-2), 82-90.
- Mathew, M. D. (2022). Nuclear energy: A pathway towards mitigation of global warming. *Progress in Nuclear Energy*, 143, 104080.
- Meleshyn, A. (2014). Microbial processes relevant for the long-term performance of high-level radioactive waste repositories in clays. *Geological Society, London, Special Publications*, 400(1), 179-194.
- Mitchell, M. J., Jensen, O. E., Cliffe, K. A., & Maroto-Valer, M. M. (2010). A model of carbon dioxide dissolution and mineral carbonation kinetics. *Proceedings of the Royal Society A: Mathematical, Physical and Engineering Sciences*, 466(2117), 1265-1290.
- Mulligan, C. N., Yong, R. N., & Fukue, M. (2009). Some effects of microbial activity on the evolution of clay-based buffer properties in underground repositories. *Applied Clay Science*, 42(3-4), 331-335.

- Nethe-Jaenchen, R., & Thauer, R. K. (1984). Growth yields and saturation constant of *Desulfovibrio vulgaris* in chemostat culture. *Archives of microbiology*, 137(3), 236-240.
- Parkhurst, D. L., & Appelo, C. A. J. (2013). Description of input and examples for PHREEQC version 3—a computer program for speciation, batch-reaction, one-dimensional transport, and inverse geochemical calculations. *US geological survey techniques and methods*, 6(A43), 497.
- Pedersen, K. (2000). *Microbial processes in radioactive waste disposal* (No. SKB-TR--00-04). Swedish Nuclear Fuel and Waste Management Co.
- Peng, D. Y., & Robinson, D. B. (1976). A new two-constant equation of state. *Industrial & Engineering Chemistry Fundamentals*, 15(1), 59-64.
- Puigdomenech, I., Ambrosi, J. P., Eisenlohr, L., Lartigue, J. E., Banwart, S. A., Bateman, K., ... & Tullborg, E. L. (2001). *O<sub>2</sub> depletion in granitic media. The Rex project* (No. SKB-TR--01-05). Swedish Nuclear Fuel and Waste Management Co..
- Ritchie, H., Rosado, P., & Roser, M. (2024). Nuclear energy. *Our World in Data*.
- Ruiz-Fresneda, M. A., Martinez-Moreno, M. F., Povedano-Priego, C., Morales-Hidalgo, M., Jroundi, F., & Merroun, M. L. (2023). Impact of microbial processes on the safety of deep geological repositories for radioactive waste. *Frontiers in Microbiology*, 14, 1134078.
- Ryu, G. W., Jang, Y. N., Bae, I. K., & Suh, Y. J. (2008). Characterization of the Kaolinite Synthesized According to the pH. *Economic and Environmental Geology*, 41(2), 165-172.
- Sawaguchi, T., Tsukada, M., Yamaguchi, T., & Mukai, M. (2016). Effects of OH<sup>-</sup> activity and temperature on the dissolution rate of compacted

- montmorillonite under highly alkaline conditions. *Clay Minerals*, 51(2), 267-278.
- Schunck, N., & Regnier, D. (2022). Theory of nuclear fission. *Progress in Particle and Nuclear Physics*, 125, 103963.
- Sin, I., De Windt, L., Banc, C., Goblet, P., & Dequidt, D. (2023). Assessment of the oxygen reactivity in a gas storage facility by multiphase reactive transport modeling of field data for air injection into a sandstone reservoir in the Paris Basin, France. *Science of the Total Environment*, 869, 161657.
- Steinmetz, D. R. (2007). *Texture evolution in processing of polystyrene-clay nanocomposites* (Doctoral dissertation, Drexel University).
- Sun, Z., Chen, Y. G., Ye, W. M., Cui, Y. J., & Wang, Q. (2020). Swelling deformation of Gaomiaozi bentonite under alkaline chemical conditions in a repository. *Engineering Geology*, 279, 105891.
- USGS. (2004). A compilation of rate parameters of water-mineral interaction kinetics for application to geochemical modeling. U.S., 2004-1068.
- Watson, C., Hane, K., Savage, D., Benbow, S., Cuevas, J., & Fernandez, R. (2009). Reaction and diffusion of cementitious water in bentonite: results of 'blind' modelling. *Applied Clay Science*, 45(1-2), 54-69.
- Wersin, P., Alt-Epping, P., & Pitkänen, P. (2014). *Sulphide fluxes and concentrations in the spent nuclear fuel repository at Olkiluoto* (No. POSIVA--14-1). Posiva Oy.
- West, J. M., Christofi, N., & McKinley, I. G. (1985). Overview of recent microbiological research relevant to the geological disposal of nuclear waste. *Radioact. Waste Manage. Nucl. Fuel Cycle;(United Kingdom)*, 6(1).
- Wikramaratna, R. S., Goodfield, M., Rodwell, W. R., Nash, P. J., & Agg, P. J. (1993). *A preliminary assessment of gas migration from the copper/steel*

*canister* (No. SKB-TR--93-31). Swedish Nuclear Fuel and Waste Management Co.

Wilson, J. C. (2017). FEBEX-DP: Geochemical Modelling of iron-Bentonite Interactions. *Quintessa's Contribution on Behalf of RWM QRS-1713A-R3, 1*, 68.

Wolery, T. J., & Sutton, M. (2013). *Evaluation of thermodynamic data* (No. LLNL-TR-640133). Lawrence Livermore National Lab.(LLNL), Livermore, CA (United States).

Ye, W. M., Cui, Y. J., Qian, L. X., & Chen, B. (2009). An experimental study of the water transfer through confined compacted GMZ bentonite. *Engineering Geology, 108*(3-4), 169-176.

Zheng, L., Rutqvist, J., Birkholzer, J. T., & Liu, H. H. (2015). On the impact of temperatures up to 200 C in clay repositories with bentonite engineer barrier systems: A study with coupled thermal, hydrological, chemical, and mechanical modeling. *Engineering Geology, 197*, 278-295.

# 사용 후 핵연료 지하 처분장 조건에서 반응성 가스-지하수-벤토나이트 시스템의 지화학 반응 모델 연구

신 대 현

부경대학교 대학원 지구환경시스템과학부

지구환경과학전공

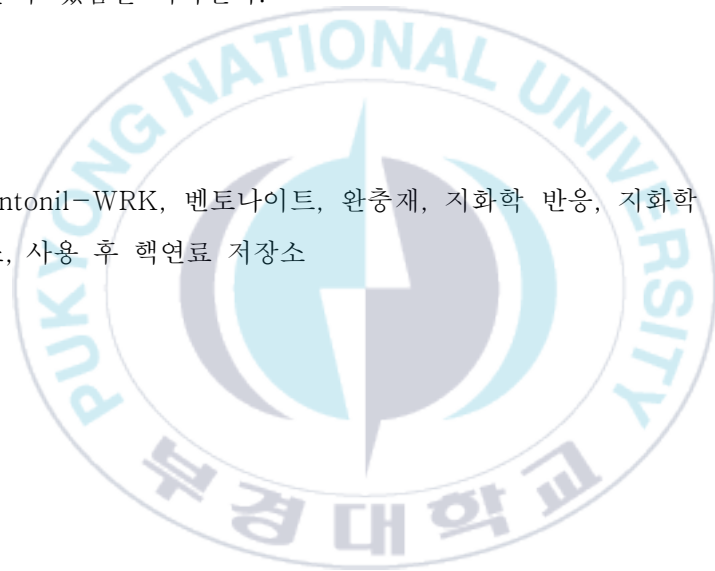
## 요약문

벤토나이트는 높은 팽윤성, 낮은 수리전도도, 방사성핵종 흡착 특성으로 인해 사용 후 핵연료(SNF) 지하 처분장에서 사용가능한 완충재 소재로 인정받고 있다. 하지만 SNF 처분장의 수리지질학적 진화 과정에서 발생하는 CO<sub>2</sub> 와 H<sub>2</sub>S 같은 반응성 가스는 완충재 소재인 벤토나이트의 화학적 및 물리적 특성을 변화시킬 수 있으며, 이는 SNF 지하 처분장의 장기 안정성에 영향을 미칠 수 있다. 본 연구에서는 반응성 가스(CO<sub>2</sub> 와 H<sub>2</sub>S)가 국내 SNF 처분장의 완충재 후보 물질인 Bentonil-WRK 의 특성에 미치는 영향을 평가하기 위해, 반응성 가스-지하수-벤토나이트 반응 시스템을 모사한 중-장기 지화학반응 모델링을 수행하였다. 지화학 반응 수치모델을 위해 PHREEQC version 3.7.3 지화학반응 코드를 사용하였으며, LLNL(Lawrence Livermore National Laboratory) 데이터베이스를 모델링을 위한 주요 열역학 데이터로 활용하였고, 실내실험과 분석을 통해 얻은 Bentonil-WRK 의 광물학적 특성자료와 KURT(KAERI Underground Research Tunnel) 지하수 샘플의 수질 데이터를 사용하였다. 본 모델 연구에서는 반응성 가스의 지화학반응, 산화환원 조건에서의 미생물 호흡, 벤토나이트 내 광물의 용해/침전 반응 등을 고려하였다.

반응 평형 모델링 결과, 벤토나이트 블록의 공극에서 잔류 대기 가스의 용해로 인해 주변 암반에서 유입된 지하수가 산성 및 호기성 환경으로 전환된 것으로 나타났다. 이후 산화환원 조건에 따라 비평형(kinetic) 지화학반응 모델링이 수행되었으며, 초기 반응단계에서는, 호기성 미생물 호흡 과정에 의해 O<sub>2</sub> 와 SO<sub>4</sub><sup>2-</sup> 이온이 소비되며 CO<sub>2</sub> 와 H<sub>2</sub>S 가스를 생성하였고, 약 5,190 년 후 완충재 영역의 호기성 환경이 혐기성 환경으로 전환되었다. 100,000 년의 지화학

반응기간 동안 Bentonil-WRK의 주요 광물인 montmorillonite와 calcite는 용해 과정에 의해 각각 0.024%와 0.37%의 질량 손실을 보였으며, kaolinite, dolomite, chalcedony, pyrite와 같은 2차 광물의 침전도 발생하였다. 100,000년의 반응 시뮬레이션 기간 동안 Bentonil-WRK의 부피는 총 0.0029%가 감소한 반면, 공극 부피는 0.0043%가 증가하였다. 이러한 결과는 100,000년에 걸친 반응 동안 반응성가스-KURT 지하수-벤토나이트 반응계에서 벤토나이트의 침전반응보다는 용해 반응이 우세하였다는 것을 보여주며, 이는 SNF 지하 처분장 환경에서 잠재적으로 생성될 수 있는 반응성 가스가 처분장의 완충재 특성에 영향을 미칠 수 있음을 시사한다.

주제어: Bentonil-WRK, 벤토나이트, 완충재, 지화학 반응, 지화학 반응 모델링, 반응성 가스, 사용 후 핵연료 저장소



## 감사의 글

3년 6개월이라는 길지만 짧은 시간을 실험실에서 보내고 석사 학위를 받아 졸업하게 되었습니다. 우선, 부족한 저를 앞으로 나아갈 수 있도록 이끌어 주시고 믿음을 주신 이민희 교수님께 진심으로 감사의 인사를 드립니다. 교수님께서 아낌없이 주신 열정과 지식으로 배움의 가치와 즐거움을 알게 되었고 석사 과정을 무사히 마칠 수 있었습니다. 교수님의 가르침과 애정을 바탕으로 성장해왔으며, 앞으로 계속해서 나아가겠습니다. 학문 뿐만 아닌 인생을 살아감에 있어서 잊지 못할 스승님이 되어 주셔서 글로는 담지 못할 만큼 감사드립니다. 그리고 바쁜 일정 속에서도 저의 논문 심사를 위해 시간을 내어 새로운 방향성과 피드백을 주신 왕수균 교수님, 김영재 교수님께도 감사의 인사를 드립니다.

연구실 생활에서 힘들 때나 기쁠 때, 언제나 저에게 힘이 되어 주시고, 따뜻한 말씀과 조언을 아끼지 않고 도와주신 한이경 박사님께 감사드립니다. 그리고 가장 가까이에서 제 미래와 연구에 대한 고민을 함께 해주시고 언제나 웃으며 환하게 반겨주신 김선옥 박사님께 감사드립니다. 그리고 힘들거나 고민이 있을 때 도와준 단우형, 언제나 고민과 웃음을 마음 놓고 나눌 수 있는 친구가 되어준 소영이, 힘든 실험실 생활에 가장 큰 힘이 되어주었던 정현이, 언제나 밝은 모습으로 챙겨주고 실험실에 와줘서 고마운 소영누나, 보기만해도 듣직하고 실험실을 위해 노력하는 원범이, 잘하고 있고 앞으로도 잘할 거라 생각되는 동준이에게 너무나도 감사합니다. 학부시절 큰 도움을 주신 경태형, 선희누나, 현지누나에게도 감사드립니다. 연구실에 들어올 수 있게 도와준 유나에게도 감사합니다. 또한 많은 조언과 격려를 해주시는 환토방 선배님들께도 감사의 인사를 전합니다. 다사다난했던 대학생월에 힘이 되어주고 함께 해준 태정누나, 주희, 대웅이, 영언이, 민지, 수빈이 모두에게 감사의 인사를 전합니다. 그리고 언제나 본일 일처럼 나서서 도와준 여지현 조교님 감사합니다.

마지막으로 하나뿐인 아들을 그 누구보다 응원하고 믿어준 우리 가족들에게 너무나 사랑하고 감사하다는 말씀을 드립니다. 지금까지 그래왔고 앞으로도 저의 축복만을 바라는 세상에 하나뿐인 우리 엄마, 아빠, 종이가 있었기 때문에 석사 과정을 무사히 마쳤습니다. 항상 너무나도 사랑하고 감사합니다. 끝으로 저를 응원하고 도움을 주신 모든 분들께 감사하다는 말씀을 전하고 싶습니다.